Combined transcriptome and proteomics analysis of yak PASMCs under hypoxia and normoxia conditions

Lan Zhang [1], **Shuwu Chen** [1, 2, 3], **Yifan Yao** [1, 2, 3], **Yiyang Zhang** [1, 2, 3], **Rui Li** [1, 2, 3], **Manlin Zhou** [1], **Zilin Qiao** [1, 2, 3], **Kun Yang** Corresp. 1, 2, 3

[1] Life Science and Engineering College, Northwest Minzu University, Lan, China

[2] Biomedical Research Center, Northwest Minzu University,, Lan Zhou, China

[3] Gansu Tech Innovation Center of Animal Cell, Gansu Tech Innovation Center of Animal Cell, Lan Zhou, China

Corresponding Author: Kun Yang
Email address: 186152592@xbmu.edu.cn

Background. Yak is a plateau animal that has resided in a plateau environment for generations. Yak can not only adapt to a plateau hypoxic environment, but also pass its adaptability to the next generation. However, the yak adaptation genes for hypoxia have not been sufficiently and comprehensively revealed. **Methods.** Pulmonary artery smooth muscle cells (PASMCs) were cultured for 72 h under hypoxic (1% O_2) and normoxic (20%O_2) conditions, and RNA-seq transcriptome analysis combined with TMT proteomics analysis was conducted. Accordingly, RNA and proteins were collected from the anoxic and normoxia groups for RNA-seq transcriptome sequencing and TMT marker protein quantification, and RT-qPCR validation was performed. **Results.** A total of 17,711 genes and 6,859 proteins were identified. Further, 5,969 differentially expressed genes and 531 differentially expressed proteins were screened owing to the comparison, including 2,924 and 186 upregulated genes and proteins and 3,045 and 345 down-regulated genes and proteins, respectively. The combination of transcriptomic and proteomic analysis revealed that 109 differentially expressed genes were highly positively correlated with differentially expressed proteins, with 77 genes showing the same expression trend. In fact, 9 overlapping genes were identified in the HIF-1 signalling pathway, Glycolysis / Gluconeogenesis, Central carbon metabolism in cancer, PPAR signalling pathway, AMPK signalling pathway, and Cholesterol metabolism (*PGAM1, PGK1, TPI1, HMOX1, IGF1R, OLR1, SCD, FABP4 and LDLR*). This finding suggests that these differentially expressed genes and protein functional classifications are related to the hypoxia-adaptive pathways. Overall, our study provides abundant data for further analysis of the molecular mechanism of yak PASMCs and the adaptive growth of the plateau animals.

Combined transcriptome and proteomics analysis of yak PASMCs under hypoxic and normoxic conditions

Lan Zhang[1], Shuwu Chen[1,2,3], Yifan Yao[1,2,3], Yiyang Zhang[1], Rui Li[1], Manlin Zhou[1], Zilin Qiao[1,2,3], Kun Yang[1,2,3,*]

[1] Life Science and Engineering College, Northwest Minzu University, Lan Zhou, Gansu province, China;

[2] Gansu Tech Innovation Center of Animal Cell, Lan Zhou, Gansu province, China;

[3] Biomedical Research Center, Northwest Minzu University, Lan Zhou, Gansu province, China

The first author
Lan Zhang, Northwest Minzu University, Lan Zhou, Gansu province, 730030, China
E-mail addresses: ZLzhanglan0508@163.com

Corresponding author
Kun Yang
Northwest Minzu University, Lan Zhou, Gansu province, 730030, China
E-mail addresses: 186152592@xbmu.edu.cn

Abstract

Background. Yak is a plateau animal that has resided in a plateau environment for generations. Yak can not only adapt to a plateau hypoxic environment, but also pass its adaptability to the next generation. However, the yak adaptation genes for hypoxia have not been sufficiently and comprehensively revealed.

Methods. Pulmonary artery smooth muscle cells (PASMCs) were cultured for 72 h under hypoxic (1% O_2) and normoxic (20%O_2) conditions, and RNA-seq transcriptome analysis combined with TMT proteomics analysis was conducted. Accordingly, RNA and proteins were collected from the anoxic and normoxia groups for RNA-seq transcriptome sequencing and TMT marker protein quantification, and RT-qPCR validation was performed.

Results. A total of 17,711 genes and 6,859 proteins were identified. Further, 5,969 differentially expressed genes and 531 differentially expressed proteins were screened owing to the comparison, including 2,924 and 186 upregulated genes and proteins and 3,045 and 345 down-regulated genes and proteins, respectively. The combination of transcriptomic and proteomic analysis revealed that 109 differentially expressed genes were highly positively correlated with differentially expressed proteins, with 77 genes showing the same expression trend. In fact, 9 overlapping genes were identified in the HIF-1 signalling pathway, Glycolysis / Gluconeogenesis, Central carbon metabolism in cancer, PPAR signalling pathway, AMPK signalling pathway, and Cholesterol metabolism (*PGAM1, PGK1, TPI1, HMOX1, IGF1R, OLR1, SCD, FABP4 and LDLR*). This finding suggests that these differentially expressed genes and protein functional classifications are related to the hypoxia-adaptive pathways. Overall, our study provides abundant data for further analysis of the molecular mechanism of yak PASMCs and the adaptive growth of the plateau animals.

Key words: Yak; PASMCs; Hypoxia; Normoxia; Transcriptome; Proteomics

Introduction

Low oxygen content is one of the main characteristics of a plateau environment. Some studies have shown that plain animals that rush into the plateau can develop heart disease and "animal chest disease." Yaks living at high altitudes for generations can adapt well to the hypoxic environment that exists at high altitudes; these animals do not develop pulmonary hypertension and pass their adaptability to the next generation through heredity. Currently, transcriptome analysis related to hypoxia adaptation in plateau animals has mainly been conducted using yak transcriptome studies, with a focus on reproduction. Studies have shown that the sensitivity of animal lung tissue to hypoxia is closely related to the content of smooth muscle on the pulmonary vascular wall; the higher the content of smooth muscle, the higher the sensitivity to hypoxia (Tucker et al., 1975). VSMCs maintain high plasticity in the pulmonary vascular system. Under normal physiological conditions, these cells maintain low proliferation, low migration and strong contractile force and express a set of specific cytoskeletal and contractile proteins. Under different environmental conditions, muscle cells re-enter the cell cycle and transform from the contractile phenotype in the differentiated state to the secretory phenotype in the dedifferentiated state. In the dedifferentiated state, PASMCs have low contractile ability and a strong ability to proliferate, migrate and secrete extracellular matrix (ECM). Therefore, further

research on the molecular mechanisms of PASMC dedifferentiation is of great importance for understanding and preventing cardiovascular diseases. PASMCs are involved in apoptosis, antioxidant activity, vascular composition, and other processes (John et al., 2019). The interaction between vascular smooth muscle cells and other cells leads to a continuous increase in vasoconstrictor forces and abnormal vascular proliferation and PASMCs involved in other diseases plays an important role in maintaining pulmonary circulation homeostasis (Tuder et al., 2013; Gao et al., 2016). However, data to justify the adaptive growth of plateau animals are insufficient. In this study, RNA-seq and TMT combined with liquid chromatography-mass spectrometry (LC-MS/MS) were used for transcriptome sequencing and proteomic analysis of PASMCs under anoxic and normoxic conditions. A further understanding of differentially expressed genes and regulatory pathways of PASMCs will provide a basis for further studies on the molecular mechanisms of PASMCs growth and a comprehensive understanding of the specificity of PASMCs in yaks.

Materials and methods

Animal ethics

All procedures in this study were performed in accordance with the guidelines for the care and use of experimental animals formulated by the Ministry of Science and Technology, PRC.

Culture of yak PASMCs

The sample was maintained in normal saline at approximately 25°C. The pulmonary artery was rinsed three time with normal saline and PBS before primary culture. Cells were divided into hypoxic (1% O_2) and normoxic (20% O_2) groups and cultured using the adherent culture method with three replicates in each group.

RNA extracted, library construction and sequencing

The cells (three replicates per group) were collected and cultured for 72 h. Briefly, the cells were collected by TRIzol lysis (6-well plate with 80 % cell density) and centrifuged at 2000 rpm for 5 min; the resulting supernatant was then discarded. TRIzol (1 mL) was added to the cell precipitates, and after thorough mixing, the sample mixture was left to stand at room temperature for 5 min and then transferred to a new 1.5 MLEP tube. Agarose gel electrophoresis was performed to determine the integrity of RNA and the presence of DNA contamination. RNA purity (OD260/280 and OD260/230 ratios) was measured using a nanophotometer spectrophotometer, and RNA integrity was accurately detected using Agilent 2100 BioAnalyzer. High-throughput sequencing was performed for library construction and quality inspection. Sequencers were used to capture fluorescence signals and a computer software was used to convert the optical signals into sequencing peaks to obtain the waiting time. The sequence information of the fragment was then measured and the raw data (raw reads) in fastq format were processed using in-house Perl scripts. In this step, clean data (clean reads) were obtained by removing reads containing adapter, poly-N, and low-quality reads from the raw data. The Q20, Q30, and GC contents of the clean data were also calculated. All downstream analyses were based on high-quality clean data. The reference genome and gene model annotation files were downloaded directly from the genome website. The index of the reference genome was built using Hisat2 v2.0.5 and clean paired-end reads were aligned to the reference genome using

Hisat2 v2.0.5. Hisat2 was selected as the mapping tool as Hisat2 can generate a database of splice junctions based on the gene model annotation file and thus provide a better mapping result than other non-splice mapping tools. featureCounts v1 .5.0-p3 was used to count the number of reads mapped to each gene. Thereafter, the FPKM of each gene was calculated based on the length of the gene and the read count mapped to this gene. FPKM, the expected number of fragments per kilobase of transcript sequence per million base pairs sequenced, considers the effect of sequencing depth and gene length for the read count. Prior to differential gene expression analysis, for each sequenced library, the read counts were adjusted by edgeR program package through one scaling normalized factor. Differential expression analysis of two conditions was performed using the edgeR R package (3.18.1). The P values were adjusted using the Benjamini & Hochberg method. Corrected P-value of 0.05 and absolute foldchange of 1 were set as the threshold for significantly differential expression. Differential expression analysis of two conditions/ groups was performed using the DESeq2 R package (1.16.1). The statistical power of this experimental design, calculated in RNASeqPower as "rnapower (821.7883585, n =3.3, cv = 0.039387208, effect=2, alpha=0.05)" is 1. (Therneau et al, 2022). (http://www.bioconductor.org/packages/release/bioc/html/RNASeqPower.html) DESeq2 provide statistical routines for determining differential expression in digital gene expression data using a model based on negative binomial distribution. The resulting P-values were adjusted using Benjamini and Hochberg's approach to control the false discovery rate. Genes with an adjusted P-value <0.05 found by DESeq2 were considered differentially expressed.

Total protein extraction and TMT quantitative proteomic analysis

Proteins were extracted by SDT lysis. Thereafter, an appropriate amount of the SDT lysate was added to the cell samples, and the cells were treated with ultrasound, boiled in a water bath for 15 min and centrifuged at 14,000 rpm for 15 min. After the supernatant was collected, the protein amount was quantified. Twenty micrograms of protein was extracted from each sample. Thereafter, 6× sample loading buffer was added to the samples, which were then bathed in boiling water for 5 min. SDS-PAGE (12%) was performed at a constant pressure of 250 V for 40 min. FASP enzymolysis was performed using samples. One hundred micrograms of peptide was collected from each sample and labelled according to the TMT labelling kit (Thermo Fisher Technologies, 90064CH). The labelled peptides were mixed and graded. The column was balanced with a 100% A solution (10 mmol L^{-1} HCOONH4, 5% ACN, pH=10.0). During the elution process, the absorption value was 214 nm and approximately 40 eluted components were collected every 1 min. The samples were lyophilised and re-dissolved in 0.1% FA into 10 parts. Each sample was separated using an Easy nLC system with a nanolitre flow rate. The original data were obtained and the blank values were removed according to the conditions of ScoreSequestHT>0 and Uniquepeptide ≥1 to screen the trusted proteins. Based on the screened trusted proteins, differentially expressed protein (DEPs) screening was carried out according to FC Fold change ≥1.3 or ≤0.78 and P<0.05. GO analysis was performed using the identified DEPs using Blast2GO software to describe the properties of the differentially expressed proteins from three aspects: biological processes, molecular functions and cellular components. The enriched DEPs were subjected to Kyoto Encyclopedia of Genes and Genomes (KEGG) pathway

analysis to identify the main signal pathways. Functional domain annotation analysis of DEPs was performed using the Interpro database.

Combined transcriptome and proteomics analysis

In the process of proteome and transcriptome analysis, the quantitative analysis results of the proteome and transcriptome were obtained, and then differentially expressed proteins and mRNA were extracted. The results of combined transcriptome and proteome analysis, were subjected to correlation clustering analysis and GO/KEGG enrichment analysis.

Results

Gene expression distribution

The sequencing depth of this experiment was 6G with three replicates per group. Owing to the influence of sequencing depth and gene length, RNA-seq gene expression values are generally not expressed by read count, but by FPKM, which has been successively corrected for sequencing depth and gene length. After the expression values of all genes in each sample (FPKM) were calculated, the distribution of gene expression levels in different samples was displayed using a box graph (Fig. 1). Based on this figure, the repeatability between parallel samples was relatively good.

Intersample correlation

The correlation of gene expression levels between samples is an important index for testing the reliability of the experiment and the rationality of sample selection. The closer the correlation coefficient is to 1, the higher the similarity of expression patterns between samples. The Encode program recommends a Pearson correlation coefficient square (R2) greater than 0.92 for ideal sampling and experimental conditions. In a specific project operation, we require an R^2 at least greater than 0.8 between biological repeat samples; otherwise, appropriate interpret of the samples or reperformance of the experiment is warranted. The correlation coefficients of samples within and between groups were calculated according to the FPKM values of all genes in each sample, and a heat map was generated to visually display the sample differences between groups and sample repetition within groups. The higher the correlation coefficient, the closer the expression pattern (Fig. 2). PASMCs showed a good correlation between biological duplicates under hypoxic and normoxic conditions, indicating the reliability of the sampling and sequencing.

Differential analysis of transcriptome sequencing gene expression

In this study, the two groups of samples were compared under hypoxic and normoxic conditions. Software combinations were compared to derive the differences in genetic screening and the threshold for DESeq2 ($|\log2(\text{FoldChange})| > 0$ & $\text{padj} <= 0.05$). A total of a total of 17,711 genes were expressed. Further, 5,969 differentially expressed genes were screened from the comparison of which 2,924 differentially up-regulated genes and 3,045 differentially down-regulated genes were selected from the comparison samples (Fig. 3A). A cluster diagram of the differentially expressed proteins (Fig. 3B) revealed that the samples under the two conditions had good biological repeatability. ClusterProfile software was used for GO functional enrichment analysis of the differentially expressed gene sets. Generally, $\text{Padj} < 0.05$ is considered to indicate significant enrichment. In Fig. 3C, the most significant 30 terms were selected to generate a bar

chart for display histograms of the biological processes, cellular components, molecular functions, and downregulation of differential genes. KEGG is a comprehensive database that integrates genomic, chemical and systemic functional information. KEGG enrichment was significantly improved with a Padj < 0.05. KEGG analysis was performed using all the differentially expressed genes, and the 20 most significant 20 KEGG pathways were selected to generated a bar chart (Fig. 3D). The differentially expressed genes were mainly enriched in the biosynthesis of amino acids, microRNAs in cancer, phagosome, human papillomavirus infection, steroid biosynthesis, Alzheimer's disease, focal adhesion., protein processing in endoplasmic reticulum, bacterial invasion of epithelial cells, colorectal cancer, fatty acid metabolism, MAPK signalling pathway, Epstein-Barr virus infection, apoptosis, AGE-RAGE signalling pathway, ECM-receptor interaction, cellular senescence, PI3K-Akt signalling pathway, pancreatic cancer, and lysosome.

Expression profiles by RT-qPCR

We selected 21 differentially expressed genes (11 down-regulated and 10 up-regulated) from the differentially expressed genes in key regulatory pathways for RT-qPCR verification (Table 3). The cells from both groups were collected and centrifuged at 2000 rpm for 5 min, and the resulting supernatant was removed. TRIzol (1 mL) was added to the cell precipitate, which was then fully mixed and allowed to stand at room temperature for 5 min. The cells were then transferred to a new 1.5 mL EP tube for total RNA extraction. cDNA was obtained by reverse transcription using the Promega M-MLV kit. Briefly, 2 μL reverse transcription primer (0.5 μg/μL) and 2.0 μg Total RNA were added to PCR tubes, with Rnase-free H2O supplemented to 11 μL. After mixing, the primer and template were centrifuged, incubated at 73.5 ℃ for 7 min, immediately placed in an ice bath and annealed. The reaction mixture (25 μL) was prepared in an ice bath (Table 4). The system was incubated in a water bath at 43.5 °C for 1 h, and then the RT enzyme was inactivated at 73.5 °C for 3 min. The cDNA of the obtained reverse transcription product was stored at -20 ℃ for future use. As shown in Table 5, a two-step proportional reaction system (12 μL) was used for RT-qPCR detection. The cycling conditions were as follows: 95 °C for 1 min, 95 °C for 10 s, 60 °C for 40 s, a total of 40 cycles. After the reaction, the final solubility curves were analysed. ACTB was used as an internal reference gene, and the relative expression levels of each gene were calculated using the $2^{-\Delta CT}$ method. RT-qPCR expression was found to be consistent with RNA-seq, and the sequencing results were confirmed to be reliable (Fig. 4).

Proteomic analysis

Based on the trusted proteins screened in the two groups, DEPs screening was performed according to FC Foldchange ≥1.3 or ≤0.78 and P<0.05. A total of 7,600 proteins were identified, including 531 differentially expressed proteins (186 up-regulated and 345 down-regulated) in the comparison group (Fig. 5A). To further understand the biological significance of DEPs under hypoxia and normoxia, DEPs enrichment was analysed using by GO functional annotation and KEGG pathway enrichment. GO enrichment analysis revealed (Fig. 5B) that the differentially expressed proteins were enriched in several categories: extracellular space, integral component of plasma membrane, cell surface, serine-type endopeptidase inhibitor activity, heparin binding,

calcium ion binding, negative regulation of endopeptidase activity, aging and neutrophil degranulation. KEGG analysis also revealed (Fig. 5C) significant DEPs enrichment in the biosynthesis of secondary metabolites, lysosome, complement and coagulation cascades, HIF-1 signalling pathway, glycolysis/gluconeogenesis, cholesterol metabolism, central carbon metabolism in cancer, PPAR signalling pathway, cytokine-cytokine receptor interaction and other glycan degradation.

Combined transcriptome and proteomics analysis

Transcriptome and proteome data were analysed from quantitative and significance viewpoints, and a Venn diagram of the differentially expressed proteins and genes in the hypoxia and normoxia groups was obtained (Fig. 6A). Combined with transcriptome, quantitative proteomics and data analysis, 109 common differential genes were identified in pulmonary smooth muscle cells under hypoxic and normoxic conditions. Significantly different proteins and genes were correlated to highlight the significance level between the different omics. The absolute value of log2FC of the transcriptome was greater than 0, and while that of the proteome log2FC was greater than 0.263, indicating an obvious trend (Fig. 6B). The horizontal and vertical coordinates in the figure represent the multiple differences (log2 value) in protein/gene expression levels in each comparison group. Red dots (opposite) indicate opposite trends in protein and transcriptome expression; blue dots (same) indicate the same trend in expression at the protein and transcriptome levels. The transcriptome had very little correlation with the proteome. Notably, the expression patterns of transcripts and proteins can be displayed more intuitively using clustering analysis. Cluster analysis was performed to derive the associations of all quantifiable/significantly different proteins and genes, and hierarchical clustering of differential proteins and associated transcriptome data was performed using a heat map (Fig. 6C). Each row in the figure represents a differentially intersected gene, and the tree structure on the left represents the aggregation of the expression patterns of differentially intersected genes. As shown in the figure, the expression levels of proteins and associated transcripts were inconsistent at both the quantifiable and significant difference levels, and certain differences were found in the expression degree and expression trend. In addition to post-transcriptional regulation, gene transcription and expression may have a certain spatial and temporal order. The significance levels of the top 10 biological process items in the transcriptome and proteomics association analysis results were analysed by GO enrichment (Fig. 6D), with the abscissa representing the significantly enriched functional items and the ordinate representing the significantly enriched significance level FDR (negative log value based on 10). In the figure, the same represents the enrichment analysis results of genes with the same expression trends in the proteome and transcriptome while the opposite represents the enrichment analysis results of genes with opposite proteome and transcriptome expression trends. Protein only indicates that there is no change in the transcriptome, and the enrichment analysis results of differentially expressed genes in the proteome only indicate the opposite pole, which represents the opposite proteome transcriptome expression trends. The protein only indicated no change in the transcriptome. Genes with similar expression trends in the proteome and transcriptomeic were mainly enriched in glycolytic process, cholesterol homeostasis, positive regulation of

inflammatory response, negative regulation of gene expression, cell migration, positive regulation of gene expression, positive regulation of cell population profile, inflammatory response, sodium transport, and epithelial cell differentiation. The same expression trend was mainly concentrated in proteolysis, signal transduction, glucose metabolic processes, fatty acid metabolic processes, positive regulation of I-kappab kinase/NF-kappab signalling, and cell adhesion. KEGG is the most commonly used authoritative database for pathway analysis. Pathway enrichment analysis results were similar to those of GO enrichment analysis; thus, by using pathway as the unit and all known genes of all genes or species on the chip as the background, the significance level of gene enrichment of each pathway was analysed and calculated by Fisher's exact test. The metabolic and signal transduction pathways were found to be significantly affected. Through KEGG pathway annotation and enrichment analysis, the significance levels of the top 10 pathways in the four types of association analysis results of the proteome and transcriptome were analysed (Fig. 6E). The abscissa represents the significantly enriched pathway, and the ordinate represents the enriched significance level FDR (negative log value based on 10). Amino acids, carbon metabolism, endocytosis, and glycolysis/gluconeogenesis were enriched by genes with the same expression trends in the proteome and transcriptome. In addition, proteoglycans in cancer, phagosome, HIF-1 signalling pathway, autophagy-animal, ovarian steroidogenesis, and other pathways were found to be enriched. Genes with opposite expression trends were mainly enriched in the lysosomal pathway.

Discussion

Transcriptome analysis of hypoxia adaptation genes in PASMCs under hypoxia and normoxia

Yaks have lived at high altitudes for generations. These animals can not only adapt well to the low-oxygen environment of the plateau, but also pass their good adaptability to the next generation. In our study, PASMCs were cultured under different conditions and their genetic differences were analysed using RNA-seq technology to provide a theoretical basis for the adaptability of plateau animals. Therefore, the characteristics of the PASMCs transcriptome under hypoxic and normoxic conditions were discussed herein, the differential genes of PASMCs were obtained, and the effects of differential genes on the adaptive growth of yaks in the plateau environment were studied. PASMCs are located in the middle membrane and are important components of the blood vessels. PASMCs play an important role in maintaining vascular morphology and tension. Under normal physiological conditions, these cells exhibit low proliferation, low migration and strong contractile forces. Under normal circumstances, PASMCs possess a contractile phenotype; however, when they are stimulated by biochemical substances and machinery, they change to a secretory phenotype, which shows decreased contractile force, enhanced migration and proliferation ability, and an enhanced ability to secrete ECM. Therefore, in this study, the characteristics of the transcriptome of PASMCs under hypoxia and normoxia were discussed. Bioinformatics shows that gene functions and their relationships can beare described from three aspects: biological processes, cell composition, and molecular function. GO functional classification annotation revealed that the differentially expressed genes were enriched in the top 30 GO categories. The main enriched biological

processes included lipid metabolic process, lipid biosynthetic processes, nucleoside metabolic processes and glycosyl compound metabolic processes. The cellular component (CC) was mainly concentrated in supramolecular complex, supramolecular polymers, supramolecular fibres and extracellular regions. Finally, the main enrich molecular functions included iron-ion binding, signalling receptor binding, hormone activity and molecular functions. KEGG enrichment pathway results showed that genes with extremely significant down-regulation differences were mainly enriched in fatty acid metabolism and the PPAR signalling pathway. Differential genes in the PPAR signalling pathway (3-hydroxy-3-methylglutaryl-coa synthase 1 (*HMGCS1*), stearoyl-CoA desaturase (*SCD*), etc.) were screened and discussed. Genes with extremely significant up-regulation differences were mainly enriched in Staphylococcus aureus infection (C3, C2 and C1s), ECM-receptor interaction and differential genes of ECM-receptor interaction (integrin alpha11 (*ITGA11*), etc.) were selected for discussion.

In this study, GO enrichment analysis showed that the upregulated differentially expressed genes under different conditions were mainly enriched in REDOX equilibrium and other biological processes or cell components. The REDOX status in smooth muscle cells is determined by reactive oxygen species (ROS), oxidation products and antioxidants. ROS are produced by the mitochondria (Tuder et al., 2013; Gao et al., 2016; Sanyour et al., 2020). In muscle cells, ROS-regulated processes include calcium homeostasis, transcriptional regulation (Hu et al., 2017), response to hypoxia and activation of apoptotic pathways. The downregulated genes were enriched in steroid biosynthesis, such as cholesterol, squalene 2,3-epoxide and cholecystalciferol biosynthesis. Cholesterol coordinates the migration and adhesion of vascular smooth muscle cells to different ECM proteins, and regulates cell hardness and cytoskeletal orientation, thereby affecting cell biomechanics (Yang et al., 2017). The pathways of glucose catabolism in the nucleoside metabolic process mainly include aerobic oxidation, anaerobic glycolysis, pentose phosphate pathway, and vascular calcification. This finding is consistent with the results of the present study, indicating that the results are reliable.

KEGG pathway is one of the most commonly used databases for annotating biological processes at the molecular level. The PPAR signalling pathway is one of the most significantly enriched KEGG pathways with down-regulated differential genes. The diversity and underestimated conserved levels of PPAR genes may lay the foundation for tumour metabolism, immunity and hypoxic survival in plateau animals. Studies have found that hypoxia further aggravates the disease phenotype of tumour subtypes with abnormal PPAR signalling (Chang & Lai, 2019). In this study, seven differentially down-regulated genes (*HMGCS1*, *SCD*, etc.) were identified in the PPAR signalling pathway. Among thes *HMGCS1* is a novel cancer marker. Zhou et al. (2020) found that *HMGCS1* can regulate the proliferation, migration and invasion of colon cancer cells, and inhibition of *HMGCS1* can completely reduce the proliferation of colon cancer cells. In a study on breast cancer, Walsh A et al. (2020) found that the down-regulation of *HMGCS1* can reduce the CSC score and function in cancer and the pharmacological inhibition of *HMGCS1* has become a treatment for breast cancer patients. A recent study showed that PE-UEXO can damage angiogenesis in human umbilical veins and endothelial cells. Microarray analysis of PE-UEXO-or exosome-treated HUVEC from normal pregnant women revealed that

the expression of *HMGCS1* in PE-UEXO-treated HUVEC was reduced. Moreover, down-regulation of *HMGCS1* in HUVEC weakens cell proliferation and migration (Ying et al., 2021). As the down-regulation of *HMGCS1* inhibits the proliferation and migration of cancer cells the inhibition of *HMGCS1* is a treatment for cancer. SCD is a key enzyme involved in the biosynthesis and regulation of unsaturated fatty acids. A remarkable feature of cancer cells is a change in lipid composition, in which monounsaturated fatty acids are significantly enriched. Increased *SCD1* expression has been observed in various cancer cells. To determine the product of *SCD1* activity and its direct influence on the tumourigenic pathway (Parajuli et al., 2017). *SCD* has become a potential new target for the treatment of various diseases, and inhibition of highly conserved *SCD* plays a significant role in the treatment of cancer (Schnittert et al., 2019). Currently, compounds that inhibit *SCD1* have been developed and clinical trials have been conducted; however, inhibition of this gene expression by hypoxia has not been reported. In this experiment, *HMGCS1* and *SCD* in PASMCS under hypoxia were significantly down-regulated genes, indicating that hypoxia could inhibit the expression of *HMGCS1* and *SCD*, but; however, the specific influencing mechanism needs further verification. Whether plateau animals can survive well in a low-oxygen environment for a long time is directly related to the down-regulation of *HMGCS1*, *SCD* and other genes and needs further verification. ECM-receptor interaction is one of the pathways that significantly enriches upregulated genes. ECM is a complex mixture of structural and functional macromolecules that play an important role in tissue and organ morphogenesis and the maintenance of cell and tissue structure and function. In addition, integrins function as mechanical receptors, providing a force-transfer physical connection between the ECM and the cytoskeleton. In this study, eight differentially expressed genes were significantly upregulated (*ITGA11*, *FN1* etc.). *ITGA11* is a collagen receptor and a coding gene of the integrin family. Himalaya Parajuli found that *ITGA11* is generally overexpressed in the stroma of squamous carcinoma of the head and neck and is positively correlated with α- smooth muscle action expression (Stribos et al., 2017). In addition, Schnittert et al. (2019) reported the overexpression of *ITGA11* in the associated fibroblasts in the stroma of pancreatic ductal adenocarcinoma, which became a target for interstitial therapy. Many studies have shown that *ITGA11* is involved in migration, epithelial-mesenchymal transformation, invasion, and metastasis in different cancers. Thus, *ITGA11* is a promising biomarker and therapeutic target and plays an important role in the regulation of cell proliferation, migration, differentiation, tumour invasion and metastasis. Prior results align with those the of the present study, indicating that the results are reliable. Whether *ITGA11* upregulation prevents cancer migration of PASMCS and is the key to the adaptive and healthy growth of yaks on the plateau requires further verification. In this study, the differential genes of PASMCs under hypoxic and normoxic conditions were evaluated to provide basis for studying the adaptive growth of yaks in plateau areas. *FN1* is a high-molecular-weight glycoprotein that exists in the animal ECM. *FN1* is a core component with complex biological functions and participates in a variety of cell biological processes, including fibrosis (Liu et al., 2020) and other diseases. *FN1* is also widely expressed in the ECM of various tumours, such as osteosarcoma, leiomyosarcoma, and gastric cancer (Tracz-Gaszewska et al., 2019). *FN1* is secreted by fibroblasts, vascular endothelial cells,

liver cells, and vascular smooth muscle cells to regulate cell adhesion, proliferation, differentiation, cell morphology maintenance, cell migration promotion, ion exchange, signal transduction, and other functions. In a recent study, *FN1* protein overexpression was reported, resulting in the deposition of the *FN1* protein in the cytoplasm of cells, ultimately affecting the normal functional activities of cells and leading to fibrosis. The more severe the bladder fibrosis, the higher the level of *FN1*. By inhibiting the synthesis of *FN1*, the fibrosis process of bladder smooth muscle cells can be reduced (Skrypek et al., 2021). *ITGA11* and *FN1* were also two of the randomly selected differentially expressed genes and the qPCR results were the same as those in this study, indicating the reliability of the results.

Proteome analysis of hypoxia adaptive proteins in PASMCs under hypoxia and normoxia

Functional enrichment and analysis of DEPs were performed using GO and KEGG, in which the HIF-1 signalling pathway, biosynthesis of secondary metabolites, central carbon metabolism in cancer, and glycolysis/gluconeogenesis extract had six important DEPs (phosphoglycerate kinase (*PGK*), hexokinases (*HK*), lactate dehydrogenase (*LDH*), phosphoglycerate Mutase (*PGAM*), phosphofructose kinase(*pfkA*) and pyruvate dehydrogenase kinase (*PDK1*)), which is the main energy supply mode under hypoxia (Table 6). PGK is an intracellular protein-and energy-producing glycolytic enzyme that catalyses the reversible transfer of 1, 3-diphosphoglycerate and ADP to produce 3-phosphoglycerate and ATP (Li et al.,2019). Under hypoxic conditions, HIF-1α up-regulates the expression of *PGK*, provides energy for the glycolysis pathway, and participates in the angiogenesis to meet the needs of body activities and adapt to the external environment (Willson et al., 2022; Duncan et al., 2022). *HK* converts glucose to glucose-6-phosphate and is a key enzyme in regulating glycolysis. The upregulation of HK under hypoxia enhances glycolysis, autophagy and epithelial-mesenchymal transformation (Chen et al., 2018). The upregulation of hexokinase can promote glycolysis by binding to withe mitochondrial outer membrane and providinge ATP for cell metabolism (Hong et al., 2021). *LDH* can be divided into LDHA and LDHB subtypes. LDHA regulates TME through HIF signalling during hypoxia. Both HIF-1α and *HIF-2α* interact with HRE-D in the *LDH* promoter to regulate *LDH* levels. LDH provides information on glycolysis levels and cellular metabolic capacity (Khan et al., 2013; Hou et al., 2020). *PGAM* is a key enzyme involved in glycolysis that can promote glycolysis by converting 3-phosphoglycerate to 2-phosphoglycerate. HIF can induce *PGAM* expression and combine with hypoxia reaction elements in the promoter region to exert transcriptional regulation, ultimately leading to an increase in *PGAM* activity (Mikawa et al., 2020). *pfkA* is Rate-limiting enzyme for enzymes involved in the cell glycolysis metabolic pathway and catalyses fructose-6-phosphate phosphorylation into fructose 1, 6 diphosphate. Recent studies have shown that *pfkA* expression is up-regulated in a low-oxygen microenvironment to promote cell metabolism and provide energy to the body. *PDK* is an important enzyme that, plays a crucial role in regulating glucose and fatty acid metabolism in the body (Di et al., 2019). Notably, HIF-1α can up-regulate the expression of *PDK1* and promote glycolysis in tumour cells (Slominski et al., 2014; Ognibene et al.,2017).

Combined analysis of hypoxia adaptive genes and proteins by PASMCs under hypoxic and

normoxic conditions

In this study, the differential genes and proteins associated with yak hypoxia adaptability were explored using combined analysis. Correlation analysis revealed 109 differentially expressed genes and proteins in PASMCs under hypoxic and normoxic conditions. Through functional enrichment and analysis of DEPs related genes by GO and KEGG (Table 7), 71 genes with the same expression trend in proteome and transcriptome were obtained; these genes were enriched in hypoxia adaptation-related pathway (HIF-1 signalling pathway, glycolysis and gluconeogenesis, central carbon metabolism in cancer, PPAR signalling pathway, AMPK signalling pathway, and cholesterol metabolism) and 9 overlapping genes were found in the pathway (*PGAM1*, *PGK1*, triosephosphate isomerase 1(*TPI1*), *HMOX1*, insulin-like growth factor 1 receptor (*IGF1R*), oxidised low-density lipoprotein receptor 1 (*OLR1*), *SCD*, fatty acid-binding protein 4(*FABP4*) and low-density lipoprotein receptor (*LDLR*)). In addition, two factors were randomly selected from the nine factors for RT-qPCR verification, and the results were consistent with the sequencing results, indicating the accuracy of the test (Fig 7). *TPI1* is key enzyme in glycolytic metabolism, is regulated by HIF-1α in hypoxic microenvironments. The expression of *TPI1* was significantly down-regulated by silt HIF-1α. In addition, Zuo et al. found that *TPI1* co-localises with HIF-1α and an interaction may exist between HIF-1α and *TPI1* (Lei et al., 2022). Haem oxygenase 1 (*HMOX1*) is a downstream target gene of HIF-1α, which is transcriptionally regulated by HIF-1α under hypoxia (Chillappagari et al., 2014). HIF-1α binds to the hypoxia response component of the *HMOXl* gene and regulates *HMOX1* expression in hypoxic response. The HIF-1α /HMOX1 pathway has been proven to be important in to alleviating lung injury (Shi et al., 2021). Han et al. (2020) and He et al. (2018) found that the activation of the HIF-1α /HMOX1 signalling pathway can improve LPS-induced acute lung injury enhance survival rate, reduce inflammation, and inhibit oxidative stress. In addition, Rashid et al. (2020) concluded that *HMOX1* is a hypoxia response gene in fish that plays a significant role in hypoxia tolerance of fish. The *IGF1R* plays a key role in cell life. *IGF1R* also plays a key role in tumour cell proliferation and apoptosis (Al-Saad et al., 2017). In recent years, relevant research has focused on the dynamic balance between *IGF1R* ubiquitination and deubiquitination (Al-Saad et al., 2017). The process of *IGF1R* ubiquitination and deubiquitination plays a key regulatory role in the survival and death of tumours. Yu et al. (2015) found that the expression level of *IGF1R* increased under hypoxia, which may lead to the synergistic stimulation of cell migration by the paracrine IGF1/ IGFIR signalling pathway. *IGF1R* was also found to be down-regulated in vivo owing to the key component of the *IGF* signalling pathway, which plays a key role in cell life activities (Yu et al., 2015). *OLR1* was first discovered in bovine aortic endothelial cells by Saamura et al. *OLR1* is mainly involved in regulating fat metabolism in the liver and mammary glands is associated with the storage of triacylglycerol, and is commonly expressed at high levels in the lungs, liver and adipose tissue (Sun et al., 2009; Cataret al.,2022). In recent years, research has mainly focused on cardiovascular and metabolic diseases, such as atherosclerosis and diabetes (Mohammed et al., 2022). In addition, numerous studies have shown that *OLR1* may be involved in the occurrence and development of cancer, especially tumour metastasis (Jiang et al. 2019). However, studies on

adaptation to hypoxia have not been conducted. *SCD* is a key rate-limiting enzyme for fatty acid synthesis and fat deposition in desaturated stearoyl-coa. Hypoxia has been found to saturate fatty acids by inhibiting *SCD*. Although oxygen (O2)-dependent *SCD* enzymes are important for cell survival, their activities can be hypoxia-limited. Therefore, hypoxia leads to the accumulation of saturated fatty acid precursors, resulting in the destruction of endoplasmic reticulum (ER) membranes and cell apoptosis. Saturated fatty acid-induced toxicity can be mitigated by the provision of exogenous unsaturated lipids, suggesting that lipid uptake is an important mechanism for maintaining a stable intracellular environment in hypoxic cells and reducing cell viability in the absence of exogenous lipid supply. *FABP4* is a member of the intracellular lipid-binding protein family. *FABP4* proteins can bind to long-chain fatty acids and play a role in fatty acid uptake, transport, and metabolism. During hypoxia, *FABP4* content increases owing to the fatty acid energy supplied. The main function of lipid partners is to actively promote lipid transport to a specific area of the cell, such as lipid drops to store the signal transmission and endoplasmic reticulum membrane synthesis of fatty acids of transshipment, besides the regulation of cell and other enzyme activity, which is the nucleus of lipid- mediated transcriptional regulation, and and participate in extracellular autocrine and paracrine effects. Lee et al. found that HIF-1α transcription-activated *FABP4* expression was increased under hypoxia. The combined activation of HIF1a and HIF1b by HIF1a enhanced *FABP4* promoter activity, and hypoxia-induced *FABP4* expression was significantly decreased under the action of HIF-1α inhibitors (Ackerman et al., 2018). *FABP4* is associated with endoplasmic reticulum stress-related apoptosis in multiple contexts. For example, *FABP4* mediates mesangial cell apoptosis via ER stress in diabetic nephropathy. Exogenous *FABP4* induces ER stress and apoptosis in liver cells. Additionally, silencing *FABP4* mitigated hypoxia/reoxygenation injury by attenuating ER stress-mediated apoptosis (Lee et al., 2017). *LDLR* is a membrane mosaic protein involved in the uptake and elimination of endogenous cholesterol. Lipid metabolism was found to be involved in the occurrence and development of hypoxic pulmonary hypertension in mice, and the down-regulation of *LDLR* gene expression under hypoxia suggests reduced cholesterol clearance and increased plasma low-density lipoprotein content in hypoxic pulmonary hypertension, suggesting that abnormal lipid metabolism is involved in the formation of hypoxic pulmonary hypertension (Gan et al., 2020).

Conclusions

In conclusion, transcriptome, proteome, and their combination analyses were used to identify possible hypoxia-adaptive genes and proteins in PASMCs under hypoxia and normoxia. This study identified overlapping genes with similar expression trends in the transcriptome and proteome, including *PGAM1*, *PGK1*, *TPI1*, *HMOX1*, *IGF1R*, *OLR1*, *SCD*, *FABP4* and *LDLR*. Our findings suggest that these differentially expressed genes and protein functional classifications are related to the hypoxia-adaptive pathways. Many issues remain to be addressed in the future, such as the mutual regulation mechanism of the hypoxia-related factors mentioned above. Nonetheless, our study provides abundant data for further analysis of the molecular mechanism of yak PASMCs and the adaptive growth of plateau animals. In addition, our study serves as a reference for the prevention and treatment of adverse reactions caused by altitude hypoxia in humans and other

animals.

Formatting of funding sources

Funding: This work was supported by National Natural Science Foundation of China [31860687]; Natural Science Foundation of Gansu Province [21JR11RA024]; The Fundamental Research Funds for the Central Universities [31920200004], and the Program for Changjiang Scholars and Innovative Research Team in the University [IRT-17R88].

Declaration of Competing InterestA

None of the authors have any conflicts of interest to declare.

Acknowledgements

We thank all contributors to the present study. This study was de-signed by Kun Yang and Lan Zhang. The manuscript was drafted by Lan Zhang and Kun Yang. Shuwu Chen, Yifan Yao, Yiyang Zhang and Rui Li helped with sample collection. Dataanalysis was performed by Lan Zhang. Zilin Qiao criticallyrevised the manuscript. All authors read and approved the final version of the manuscript.

REFERENCES

Al-Saad S, Richardsen E, Kilvaer TK, et al. 2017. The impact of MET, IGF-1, IGF1R expression and EGFR mutations on survival of patients with non-small-cell lung cancer. PLoS One 12(7): 0181527. doi: 10.1371/journal.pone.0181527.

Ackerman D, Tumanov S, Qiu B, et al. 2018. Triglycerides Promote Lipid Homeostasis during Hypoxic Stress by Balancing Fatty Acid Saturation. Cell Rep 24(10):2596-2605.e5. doi: 10.1016/j.celrep.2018.08.015.

Catar R, Chen L, Zhao H, et al. 2022. Native and Oxidized Low-Density Lipoproteins Increase the Expression of the LDL Receptor and the LOX-1 Receptor, *Respectively, in Arterial Endothelial Cells.* Cells 11(2):204. doi: 10.3390/cells11020204.

Chang WH, Lai AG.2019. The pan-cancer mutational landscape of the PPAR pathway reveals universal patterns of dysregulated metabolism and interactions with tumor immunity and hypoxia. *Annals of the New York Academy of Sciences* 1448(1):65-82. doi: 10.1111/nyas.14170.

Chen G, Zhang Y, Liang J, 2018. Deregulation of Hexokinase II Is Associated with Glycolysis, Autophagy, and the Epithelial-Mesenchymal Transition in Tongue Squamous Cell Carcinoma under Hypoxia. *Biomed Res Int* 2018:8480762. doi: 10.1155/2018/8480762.

Chillappagari S, Venkatesan S, Garapati V, et al. 2014. Impaired TLR4 and HIF expression in cystic fibrosis bronchial epithelial cells downregulates hemeoxygenase-1 and alters iron homeostasis in vitro. *Am J Physiol Lung Cell Mol Physiol.* 307(10): L791-9. doi: 10.1152/ajplung.00167.2014.

Di R, Yang Z, Xu P, et al. 2019. Silencing PDK1 limits hypoxia-induced pulmonary arterial hypertension in mice via the Akt/p70S6K signaling pathway. *Exp Ther Med* 18(1):699-704. doi: 10.3892/etm.2019.7627.

Duncan L, Shay C, Teng Y, et al.2022. PGK1: An Essential Player in Modulating Tumor Metabolism. *Methods Mol Biol.* 2343:57-70. doi: 10.1007/978-1-0716-1558-4_4.

Gan ES, Tan HC, Le DHT, et al. 2020. Dengue virus induces PCSK9 expression to alter antiviral

responses and disease outcomes. *J Clin Invest* 130(10):5223-5234. doi: 10.1172/JCI137536.
Gao YS, Chen TJ, Raj JU. 2016. Endothelial and Smooth Muscle Cell Interactions in the Pathobiology of Pulmonary Hypertension. *American journal of respiratory cell and molecular biology* 54(4):451-60. doi: 10.1165/rcmb.2015-0323TR.
Han F, Wu G, Han S, et al. 2020. Hypoxia-inducible factor prolyl-hydroxylase inhibitor roxadustat (FG-4592) alleviates sepsis-induced acute lung injury. *Respir Physiol Neurobiol* 281:103506. doi: 10.1016/j.resp.2020.103506.
Harrison PT, Vyse S, Huang PH, et al. 2020. Rare epidermal growth factor receptor (EGFR) mutations in non-small cell lung cancer. *Semin Cancer Biol* 61:167-179. doi: 10.1016/j.semcancer.2019.09.015.
He C, Zhang W, Li S, et al. 2018. Edaravone Improves Septic Cardiac Function by Inducing an HIF-1α/HO-1 Pathway. *Oxid Med Cell Longev* 2018:5216383. doi: 10.1155/2018/5216383.
Hong C, Zhuang H, Cai B, et al. 2021. β-Elemene Attenuates Fibrosis after Esophageal Endoscopic Submucosal Dissection via Modulating the HIF-1α/HK2/p38-MAPK Signaling Axis. *ACS Biomater Sci Eng* 7(7):3399-3408. doi: 10.1021/acsbiomaterials.1c00047.
Hou T, Ma H, Wang H, et al. 2020. Sevoflurane preconditioning attenuates hypoxia/reoxygenation injury of H9c2 cardiomyocytes by activation of the HIF-1/PDK-1 pathway. *PeerJ.* 2020 Dec 21;8:e10603. doi: 10.7717/peerj.10603.
Hu B, Guo Y, Garbacz WG, et al. 2015. Fatty acid binding protein-4 (FABP4) is a hypoxia inducible gene that sensitizes mice to liver ischemia/reperfusion injury. *J Hepatol* 63(4):855-62. doi: 10.1016/j.jhep.2015.05.030.
Hu H, Ding Y, Wang Y, et al. 2017. MitoKATP channels promote the proliferation of hypoxia human pulmonary artery smooth muscle cells via the ROS/HIF/miR-210/ISCU signaling pathway. *Experimental and therapeutic medicine* 14(6):6105-6112. doi: 10.3892/etm.2017.5322.
Jiang L, Jiang S, Zhou W, et al. 2019. Oxidized low density lipoprotein receptor 1 promotes lung metastases of osteosarcomas through regulating the epithelial-mesenchymal transition. *J Transl Med* 17(1):369. doi: 10.1186/s12967-019-2107-9.
John C, Huetsch, Karthik S, 2019. Regulation of Smooth Muscle Cell Proliferation by NADPH Oxidases in Pulmonary Hypertension. *Antioxidants* 8(3):56. doi: 10.3390/antiox8030056.
Khan J, Nordback I, Sand J, et al. 2013 Serum lipid levels are associated with the severity of acute pancreatitis. *Digestion* 87(4):223-8. doi: 10.1159/000348438.
Lee YS, Kim JY, Oh KS, et al. 2017. Fatty acid-binding protein 4 regulates fatty infiltration after rotator cuff tear by hypoxia-inducible factor 1 in mice. *J Cachexia Sarcopenia Muscle* 8(5):839-850. doi: 10.1002/jcsm.12203.
Lei M, Tao MQ, Wu YJ, et al. 2022. Metabolic Enzyme Triosephosphate Isomerase 1 and Nicotinamide Phosphoribosyltransferase, Two Independent Inflammatory Indicators in Rheumatoid Arthritis: Evidences From Collagen-Induced Arthritis and Clinical Samples. *Front Immunol* 12:795626. doi: 10.3389/fimmu.2021.795626.
Love MI, Huber W, Anders S. Moderated estimation of fold change and dispersion for RNA-seq data with DESeq2. Genome Biol. 2014;15(12):550. doi: 10.1186/s13059-014-0550-8.

Li FX, Zhang YS, Yao CL,2019. Characterization and role of PGK from Litopenaeus vannamei in WSSV infection. Fish Shellfish Immunol 93:144-152. doi: 10.1016/j.fsi.2019.07.048.
Liu B, Ding Y, Li P, et al. 2020. MicroRNA-219c-5p regulates bladder fibrosis by targeting FN1. *BMC Urol* 2020 Dec 7;20(1):193. doi: 10.1186/s12894-020-00765-5.
Mikawa T, Shibata E, Shimada M, et al. 2020. Phosphoglycerate Mutase Cooperates with Chk1 Kinase to Regulate Glycolysis. 23(7):101306. doi: 10.1016/j.isci.2020.101306.
Mohammed HSE, Kamal MM, ElBadre HM, et al. 2022. Lectin-Like OLR1 3'UTR Rs1050286 Gene Polymorphism and Plasma Oxidized-LDL in Coronary Artery Disease and Their Relation to Cardiovascular Risk and Outcomes. *Rep Biochem Mol Biol* 10(4):537-553. doi: 10.52547/rbmb.10.4.537.
Ognibene M, Cangelosi, D, Morini M, et al. 2017. Immunohistochemical analysis of PDK1, PHD3 and HIF-1α expression defines the hypoxic status of neuroblastoma tumors. *PLoS One* 12(11): e0187206. doi: 10.1371/journal.pone.0187206.
Parajuli H, Teh MT, Abrahamsen S, et al. 2017. Integrin α11 is overexpressed by tumour stroma of head and neck squamous cell carcinoma and correlates positively with alpha smooth muscle actin expression. *J Oral Pathol Med* 46(4):267-275. doi: 10.1111/jop.12493.
Rashid I, Baisvar VS, Singh M, et al. 2020. Isolation and characterization of hypoxia inducible heme oxygenase 1 (HMOX1) gene in Labeo rohita. *Genomics* 112(3):2327-2333. doi: 10.1016/j.ygeno.2020.01.004.
Sanyour HJ, Li N, Rickel AP, et al. 2020. Statin-mediated cholesterol depletion exerts coordinated effects on the alterations in rat vascular smooth muscle cell biomechanics and migration. *J Physiol* 598(8):1505-1522. doi: 10.1113/JP279528.
Schnittert J, Bansal R, Mardhian DF, et al. 2019. Integrin α11 in pancreatic stellate cells regulates tumor stroma interaction in pancreatic cancer. *FASEB J* 33(5):6609-6621. doi: 10.1096/fj.201802336R.
Schnittert J, Bansal R, Mardhian DF, et al. 2019. Integrin α11 in pancreatic stellate cells regulates tumor stroma interaction in pancreatic cancer. *FASEB J* 33(5):6609-6621. doi: 10.1096/fj.201802336R.
Shi J, Yu T, Song K, et al. 2021. Dexmedetomidine ameliorates endotoxin-induced acute lung injury in vivo and in vitro by preserving mitochondrial dynamic equilibrium through the HIF-1a/HO-1 signaling pathway. *Redox Biol* 41:101954. doi: 10.1016/j.redox.2021.101954.
Skrypek K, Balog S, Eriguchi Y, et al.2021. Inhibition of Stearoyl-CoA Desaturase Induces the Unfolded Protein Response in Pancreatic Tumors and Suppresses Their Growth. *Pancreas* 2021 Feb 1;50(2):219-226. doi: 10.1097/MPA.0000000000001737.
Slominski A, Kim TK, Arożyna A, et al. 2014. The role of melanogenesis in regulation of melanoma behavior: melanogenesis leads to stimulation of HIF-1α expression and HIF-dependent attendant pathways. *Arch Biochem Biophys* 563:79-93. doi: 10.1016/j.abb.2014.06.030.
Stribos EGD, Seelen MA, Goor H, et al. 2017. Murine Precision-Cut Kidney Slices as an ex vivo Model to Evaluate the Role of Transforming Growth Factor-β1 Signaling in the Onset of Renal Fibrosis. *Front Physiol* 8:1026. doi: 10.3389/fphys.2017.01026.

638 Sun C, Liu C, Zhang Z. 2009. Cloning of OLR1 gene in pig adipose tissue and preliminary study
639 on its lipid accumulating effect. *Asian Australas J Anim* 22:1420-1428.
640 Tracz-Gaszewska Z, Dobrzyn P, 2019. Stearoyl-CoA Desaturase 1 as a Therapeutic Target for
641 the Treatment of Cancer. *Cancers (Basel)* 11(7):948. doi: 10.3390/cancers11070948.
642 Tucker A, McMurtry IF, Reeves JT et al. 1975. Grover. Lung vascular smooth muscle as a
643 determinant of pulmonary hypertension at high altitude. *AJP Legacy Content* 228(3):762-7.
644 doi: 10.1152/ajplegacy.1975.228.3.762.
645 Tuder RM, Archer SL, Dorfmüller P, et al. 2013. Relevant issues in the pathology and
646 pathobiology of pulmonary hypertension. *J Am Coll Cardiol* 24;62(25 Suppl): D4-12. doi:
647 10.1016/j.jacc.2013.10.025.
648 Therneau T, Hart S, Kocher J 2022. Calculating samples: Size estimates for RNA Seq studies. R
649 package version 1.36.0.
650 Walsh CA, Akrap N, Garre E, et al. 2020.The mevalonate precursor enzyme HMGCS1 is a novel
651 marker and key mediator of cancer stem cell enrichment in luminal and basal models of
652 breast cancer. *PLoS One* 21;15(7): e0236187. doi: 10.1371/journal.pone.0236187.
653 Willson JA, Arienti S, Sadiku P, et al. 2022. Neutrophil HIF-1α stabilization is augmented by
654 mitochondrial ROS produced via the glycerol 3-phosphate shuttle. *Blood* 2022 Jan
655 13;139(2):281-286. doi: 10.1182/blood.2021011010.
656 Yang M, Chadwick AE, Dart C, et al. 2017. Bioenergetic profile of human coronary artery
657 smooth muscle cells and effect of metabolic intervention. *PLoS One* 19;12(5): e0177951.
658 doi: 10.1371/journal.pone.0177951.
659 Ying X, Zhu Y, Jin X, et al. 2021. Umbilical cord plasma-derived exosomes from preeclamptic
660 women induce vascular dysfunction by targeting HMGCS1 in endothelial cells. *Placenta*
661 103:86-93. doi: 10.1016/j.placenta.2020.10.022.
662 Yu J, Wang L, Zhang T, et al. 2015. Co-expression of β-arrestin1 and NF-κB is associated with
663 cancer progression and poor prognosis in lung adenocarcinoma. Tumour Biol 36(8):6551-8.
664 doi: 10.1007/s13277-015-3349-7.
665 Zhou S, Xu H, Tang Q, et al. 2020. Dipyridamole Enhances the Cytotoxicities of Trametinib
666 against Colon Cancer Cells through Combined Targeting of HMGCS1 and MEK Pathway.
667 *Molecular cancer therapeutics Mol Cancer Ther* 19(1):135-146. doi: 10.1158/1535-7163.
668 MCT-19-0413.

Figure 1

Figure1 Box diagram of gene expression level distribution in samples

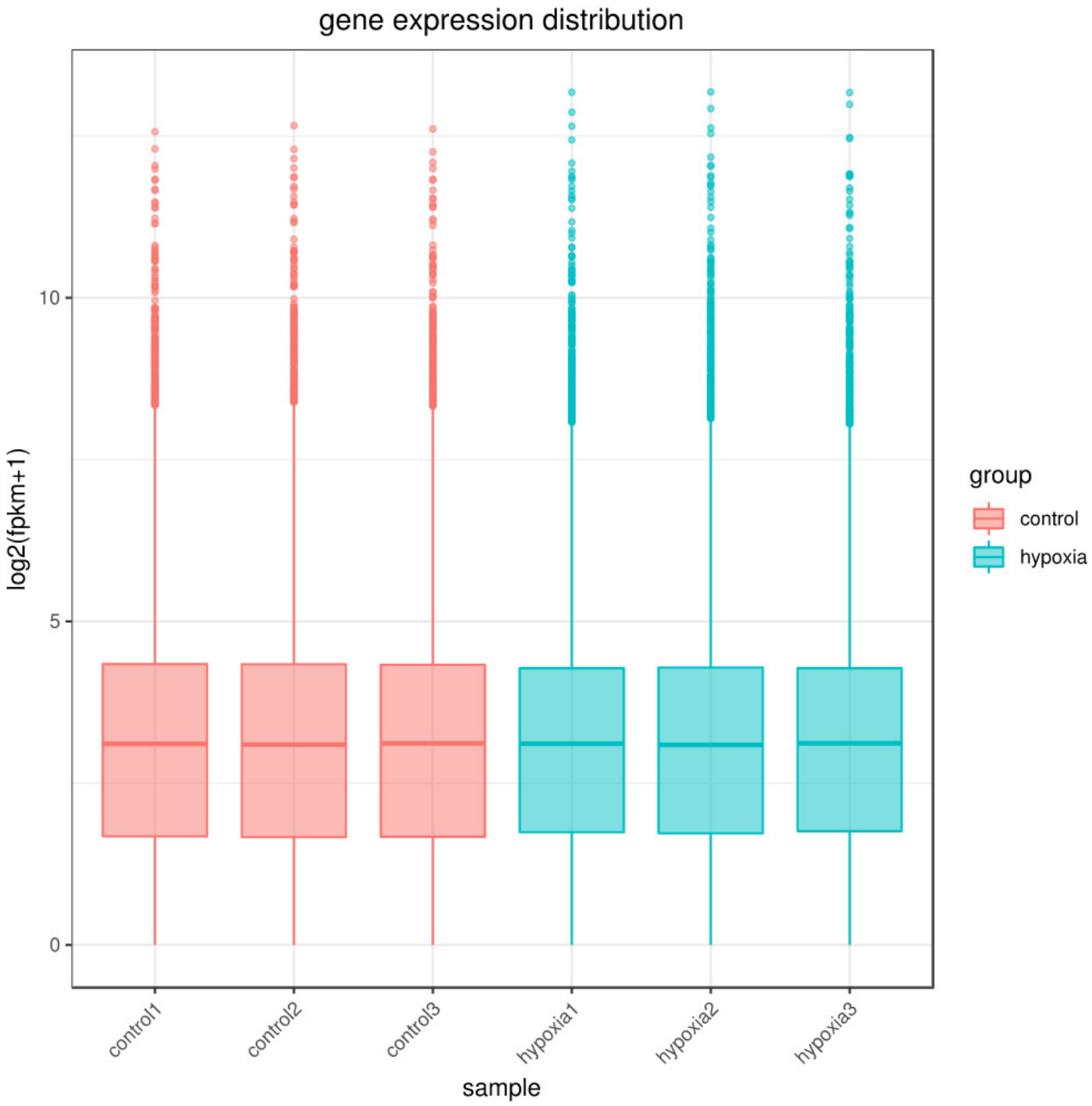

Figure 2

Figure 2 Heat map of correlation between samples

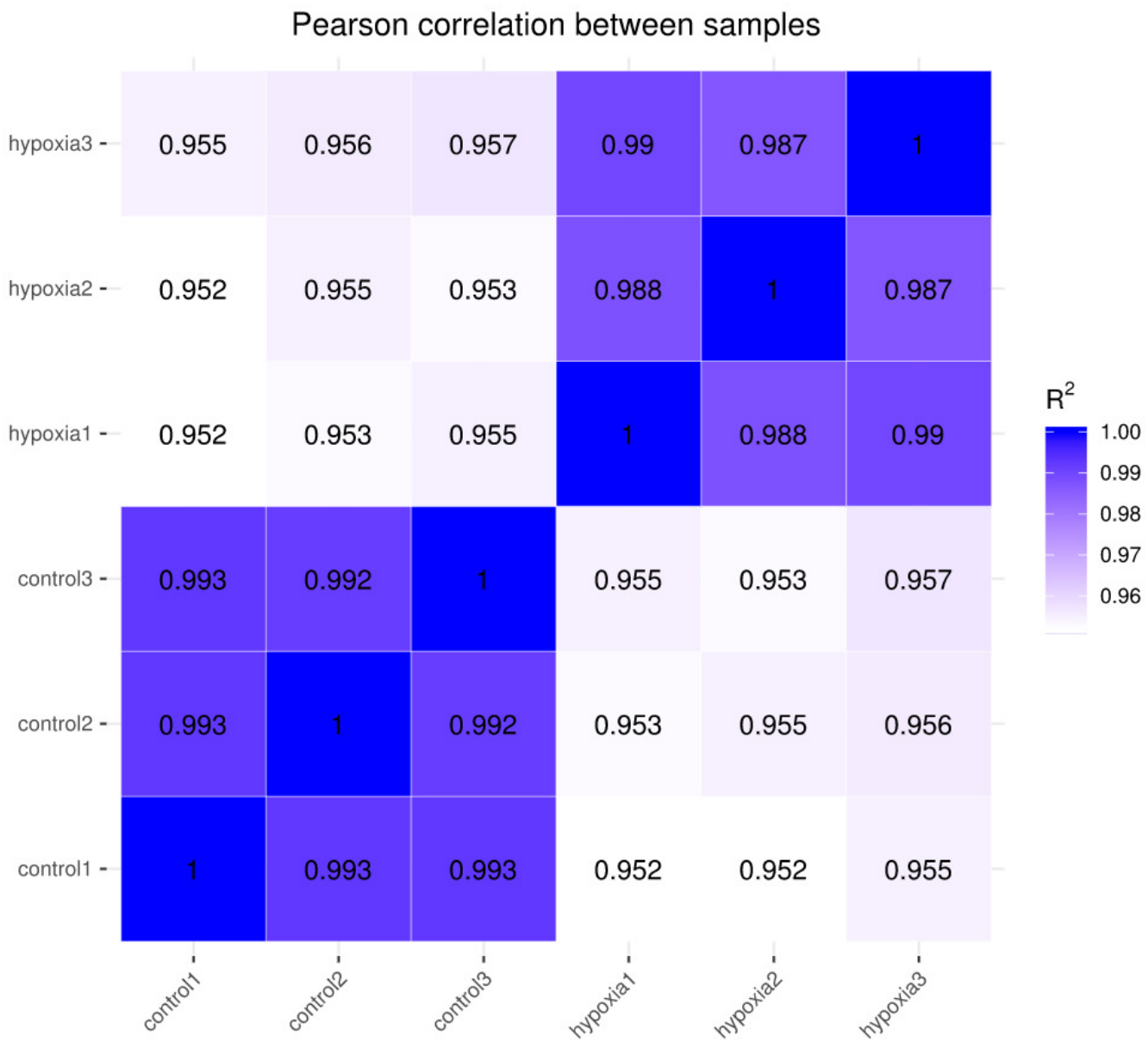

Figure 3

Figure 3A Differential gene volcano map

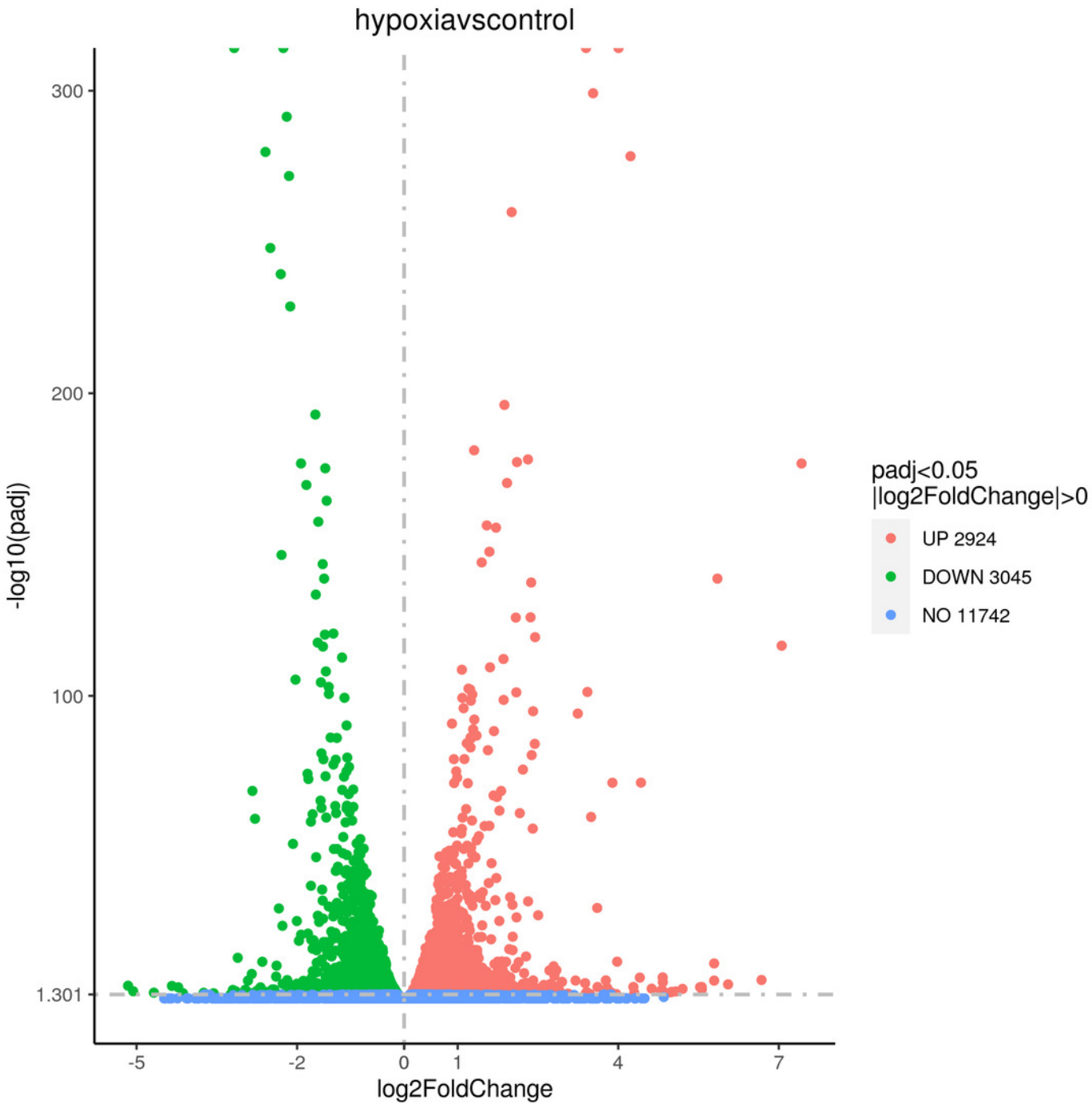

Figure 4

Figure 3B Cluster heat map of differentially expressed genes

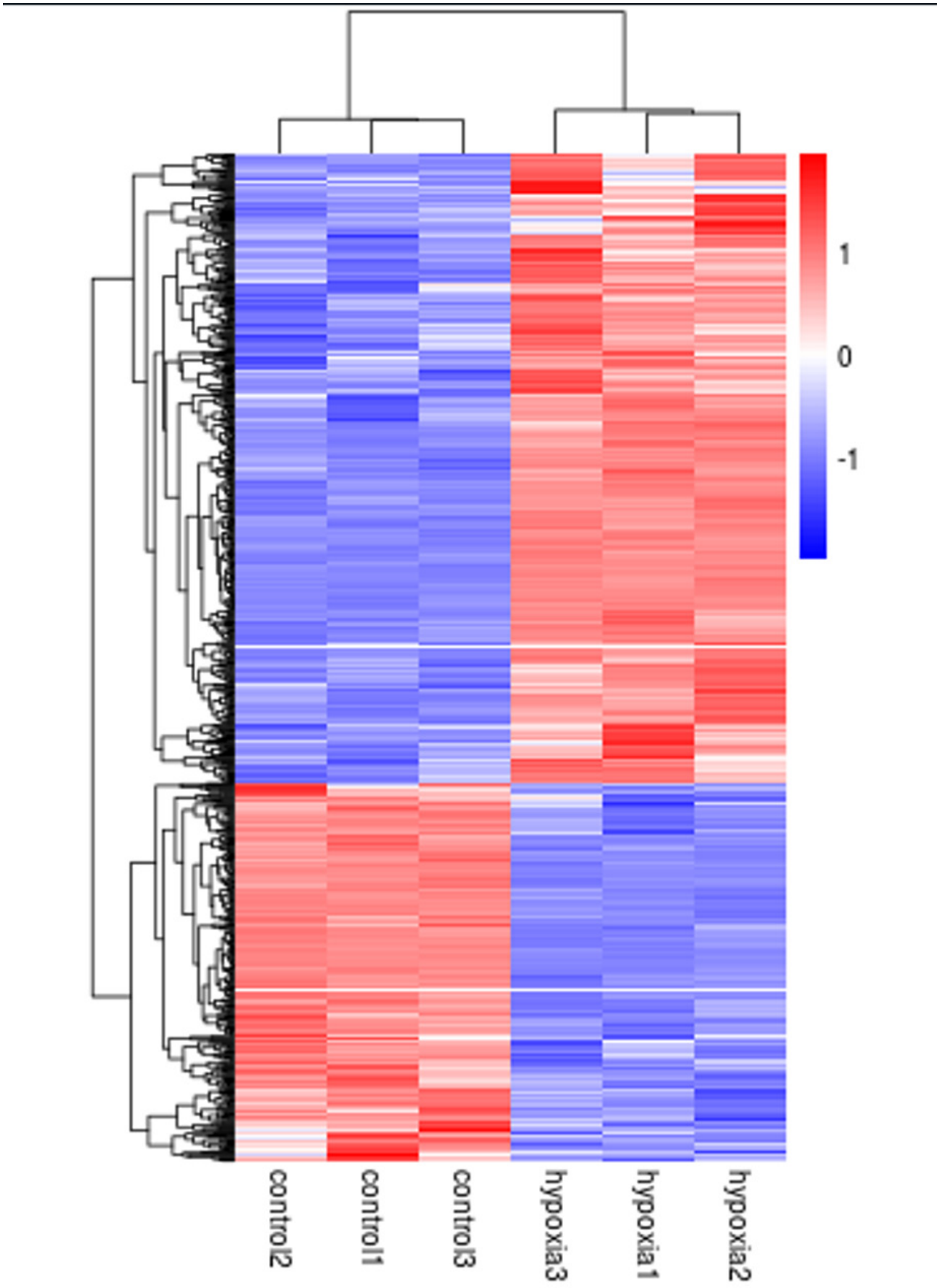
1
0
-1
control2
control1
control3
hypoxia3
hypoxia1
hypoxia2

Figure 5

Figure 3C Histogram of analysis 30 Term before GO enrichment

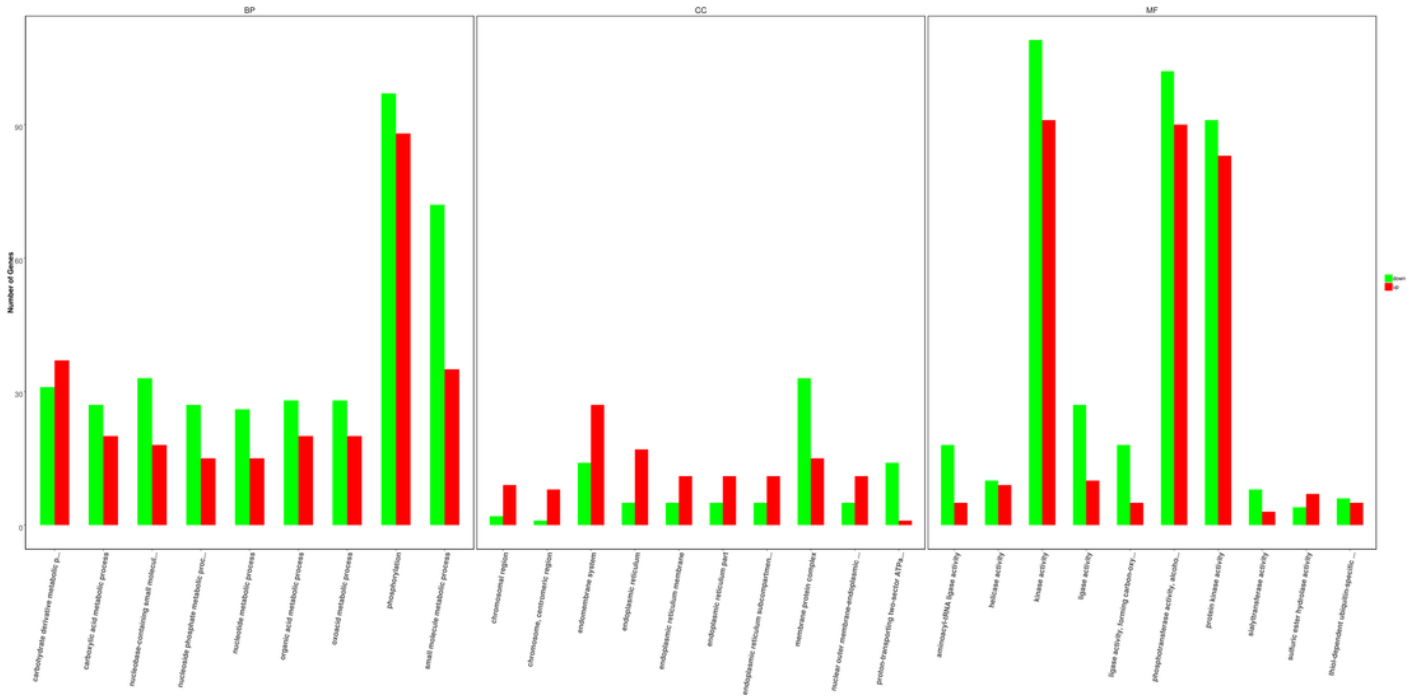

Figure 6

Figure 3D KEGG rich distribution point diagram

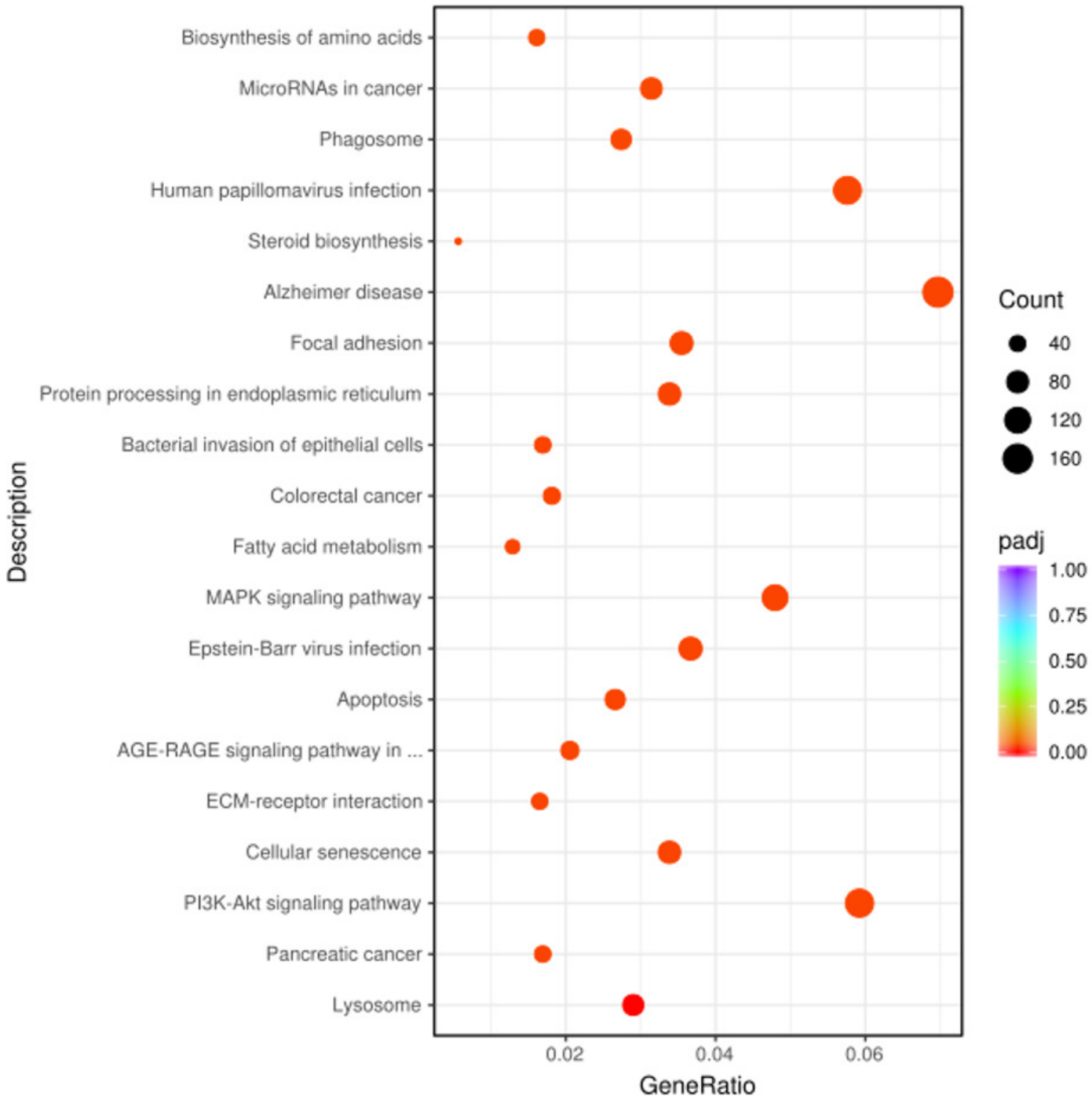

Figure 7

Figure 4 Transcriptome sequencing was verified by qRT-PCR. (A) up-regulated differential gene sequencing for qRT-PCR verification. (B) Verification by qRT-PCR with down-regulated sequencing of differential genes.

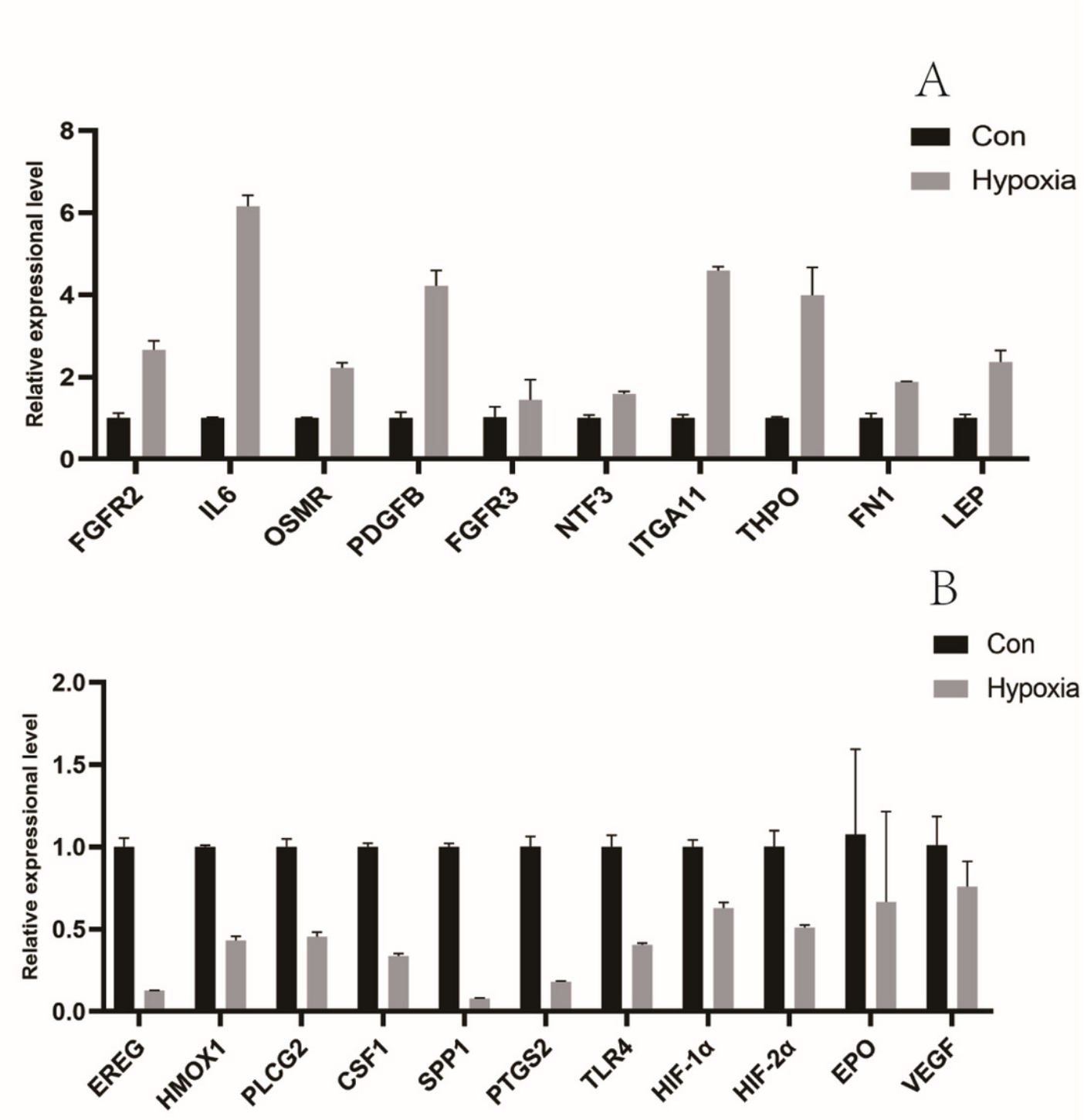
A
Con
Hypoxia
Relative expressional level
8
6
4
2
0
FGFR2
IL6
OSMR
PDGFB
FGFR3
NTF3
ITGA11
THPO
FN1
LEP
B
Con
Hypoxia
Relative expressional level
2.0
1.5
1.0
0.5
0.0
EREG
HMOX1
PLCG2
CSF1
SPP1
PTGS2
TLR4
HIF-1α
HIF-2α
EPO
VEGF

Figure 8

Figure 5 Proteomic analysis （A）Expression and distribution of DEPs (B) Enrichment analysis of GO function of DEPs.(C) Pathway enrichment analysis of DEPs .

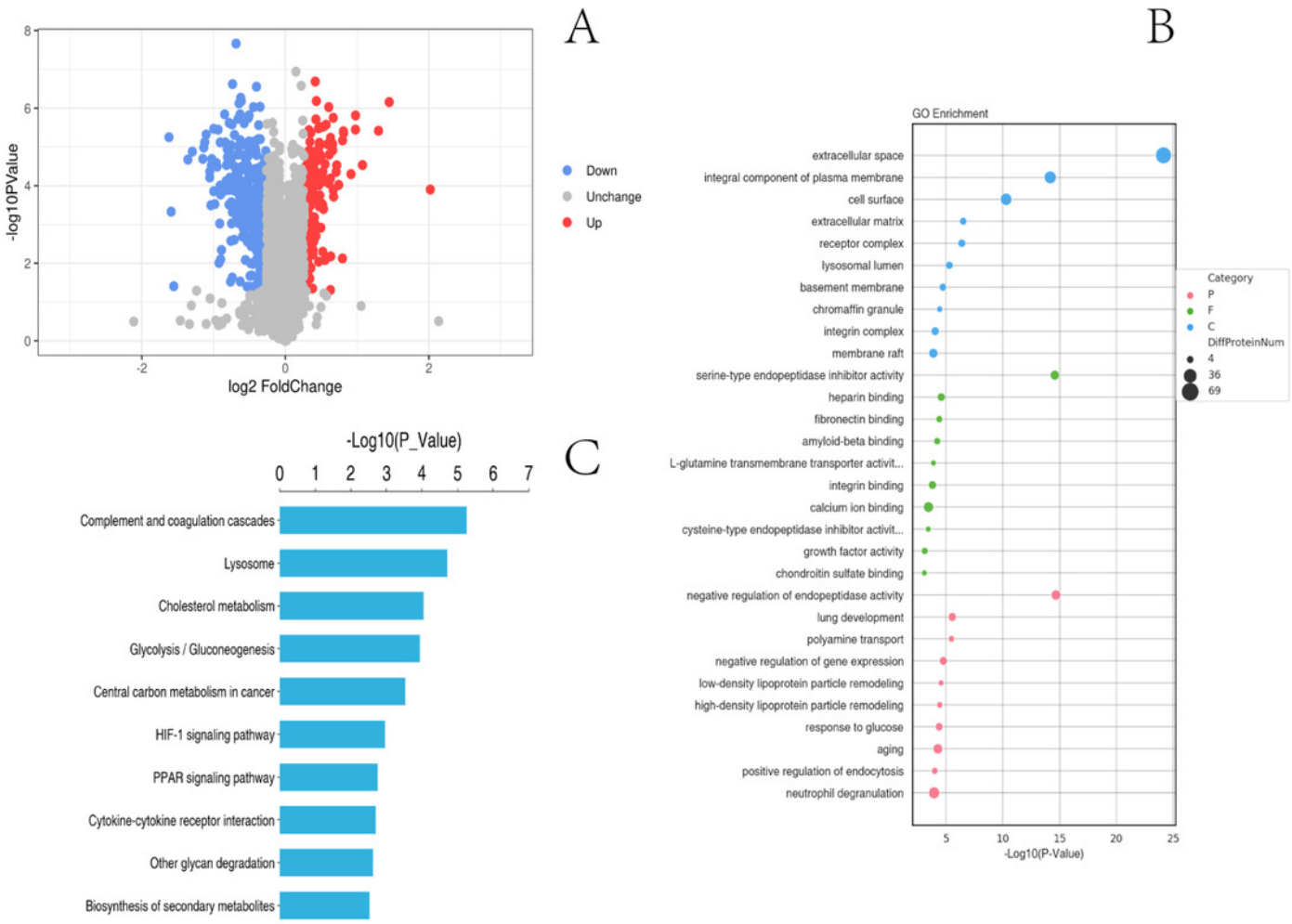

Figure 9

Figure 6A Statistics of correlation Number Venn□hypoxia VS control□

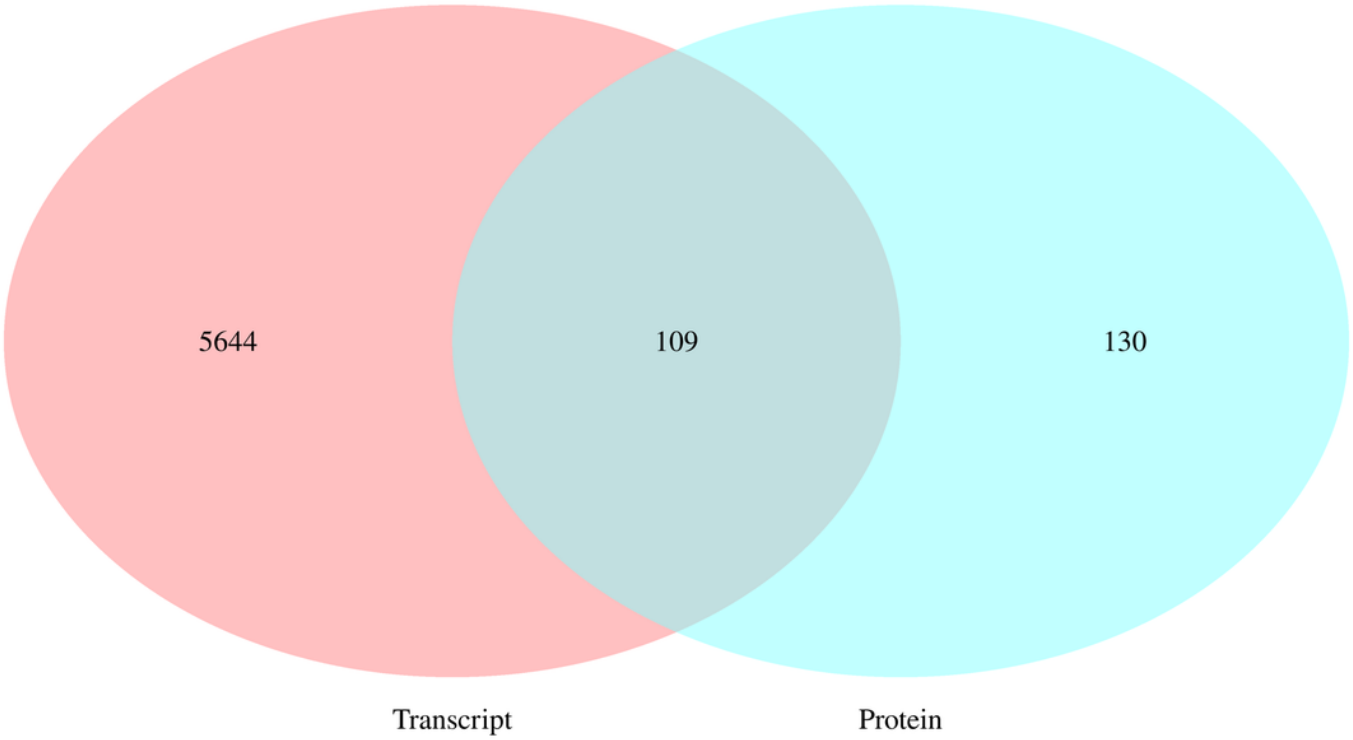

Figure 10

Figure 6B Correlation analysis between the ex pression levels of all significantly different proteins and their associated gene

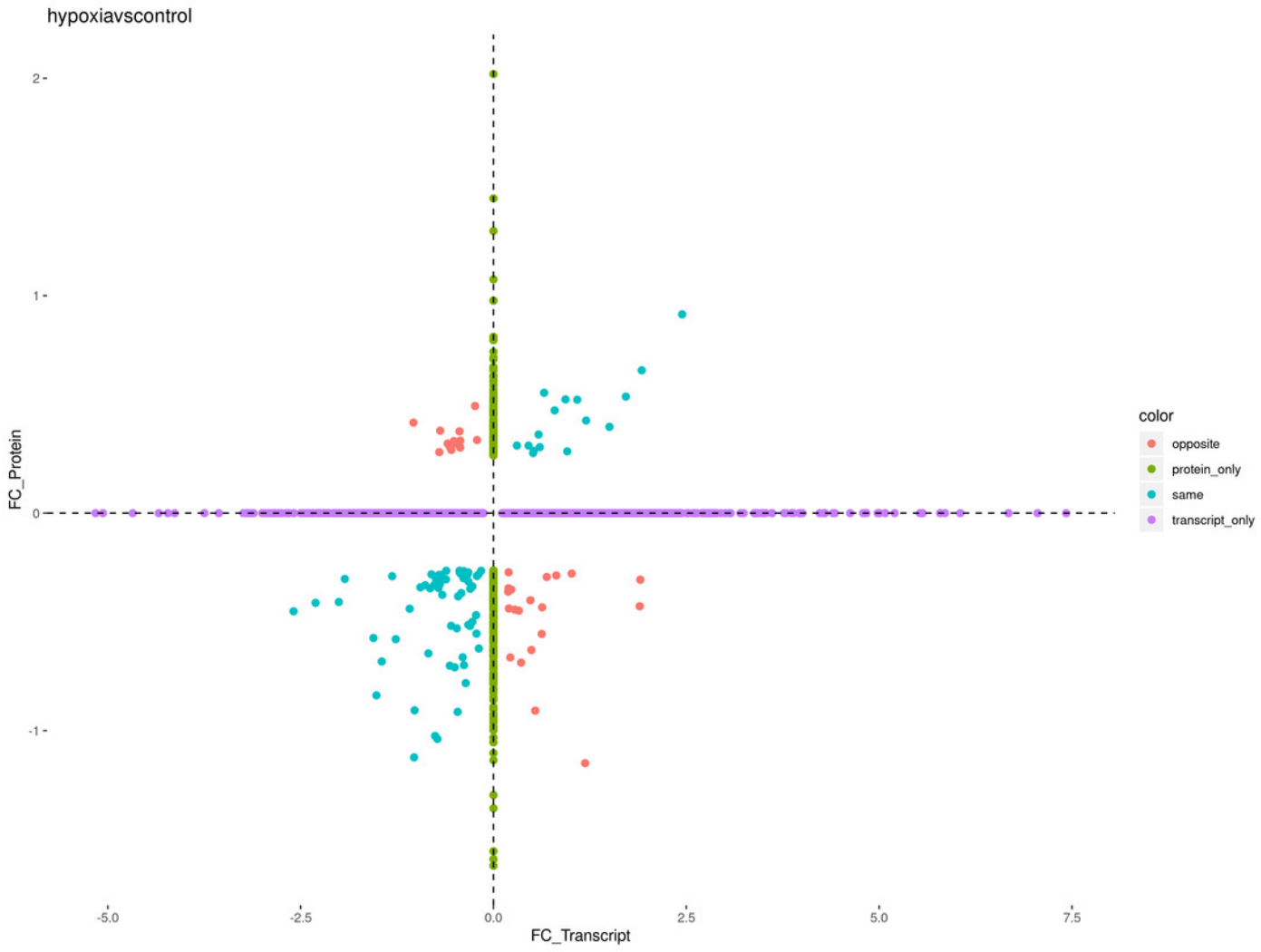

Figure 11

Figure 6C Cluster analysis between the expression levels of significantly different proteins and their associated genes

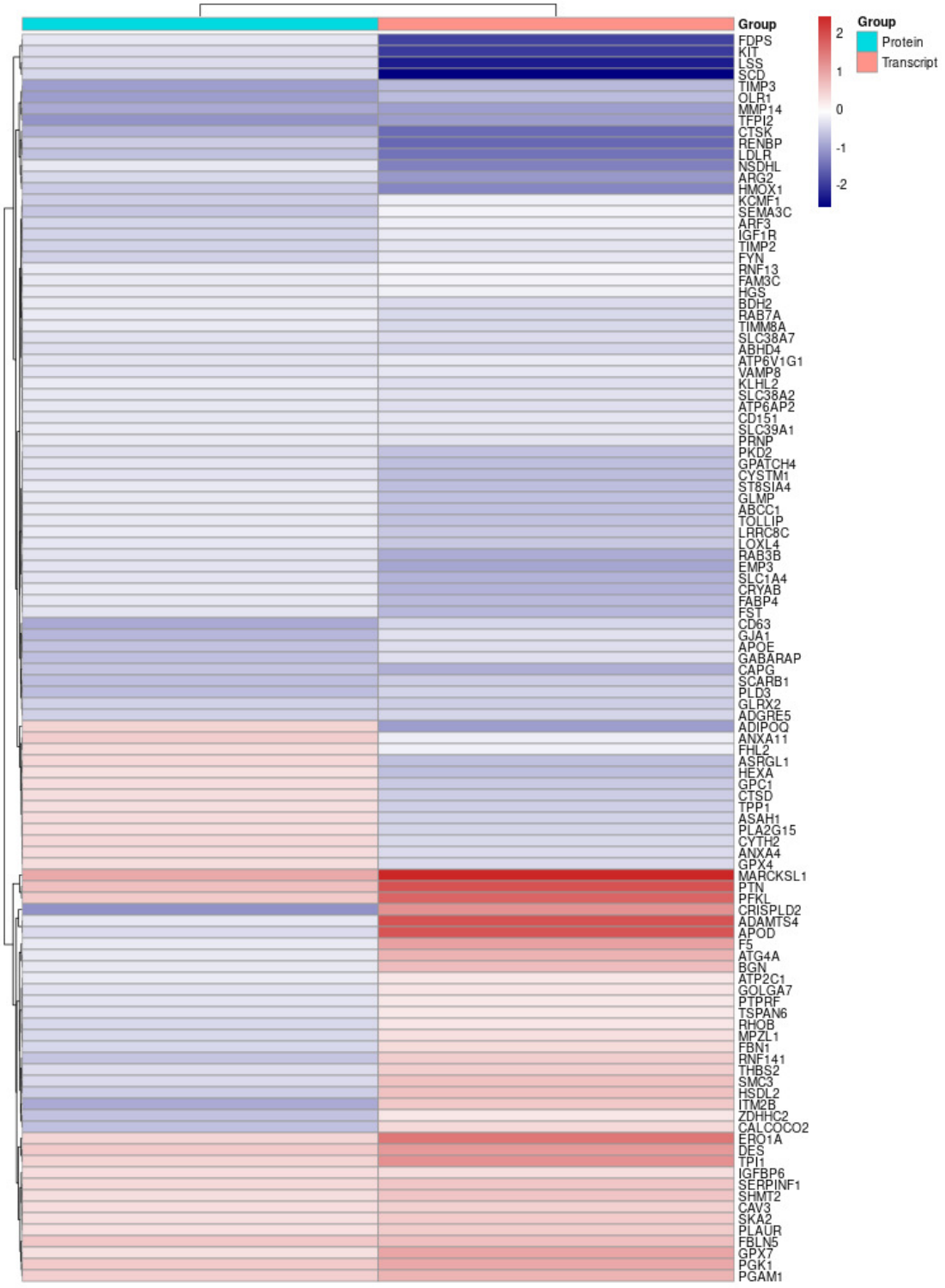
Group
FDPS
KIT
LSS
SCD
TIMP3
OLR1
MMP14
TFPI2
CTSK
RENBP
LDLR
NSDHL
ARG2
HMOX1
KCMF1
SEMA3C
ARF3
IGF1R
TIMP2
FYN
RNF13
FAM3C
HGS
BDH2
RAB7A
TIMM8A
SLC38A7
ABHD4
ATP6V1G1
VAMP8
KLHL2
SLC38A2
ATP6AP2
CD151
SLC39A1
PRNP
PKD2
GPATCH4
CYSTM1
ST8SIA4
GLMP
ABCC1
TOLLIP
LRRC8C
LOXL4
RAB3B
EMP3
SLC1A4
CRYAB
FABP4
FST
CD63
GJA1
APOE
GABARAP
CAPG
SCARB1
PLD3
GLRX2
ADGRE5
ADIPOQ
ANXA11
FHL2
ASRGL1
HEXA
GPC1
CTSD
TPP1
ASAH1
PLA2G15
CYTH2
ANXA4
GPX4
MARCKSL1
PTN
PFKL
CRISPLD2
ADAMTS4
APOD
F5
ATG4A
BGN
ATP2C1
GOLGA7
PTPRF
TSPAN6
RHOB
MPZL1
FBN1
RNF141
THBS2
SMC3
HSDL2
ITM2B
ZDHHC2
CALCOCO2
ERO1A
DES
TPI1
IGFBP6
SERPINF1
SHMT2
CAV3
SKA2
PLAUR
FBLN5
GPX7
PGK1
PGAM1
Group
2
1
0
-1
-2
Group
Protein
Transcript

Figure 12

Figure 6D Enrichment associated GO terms

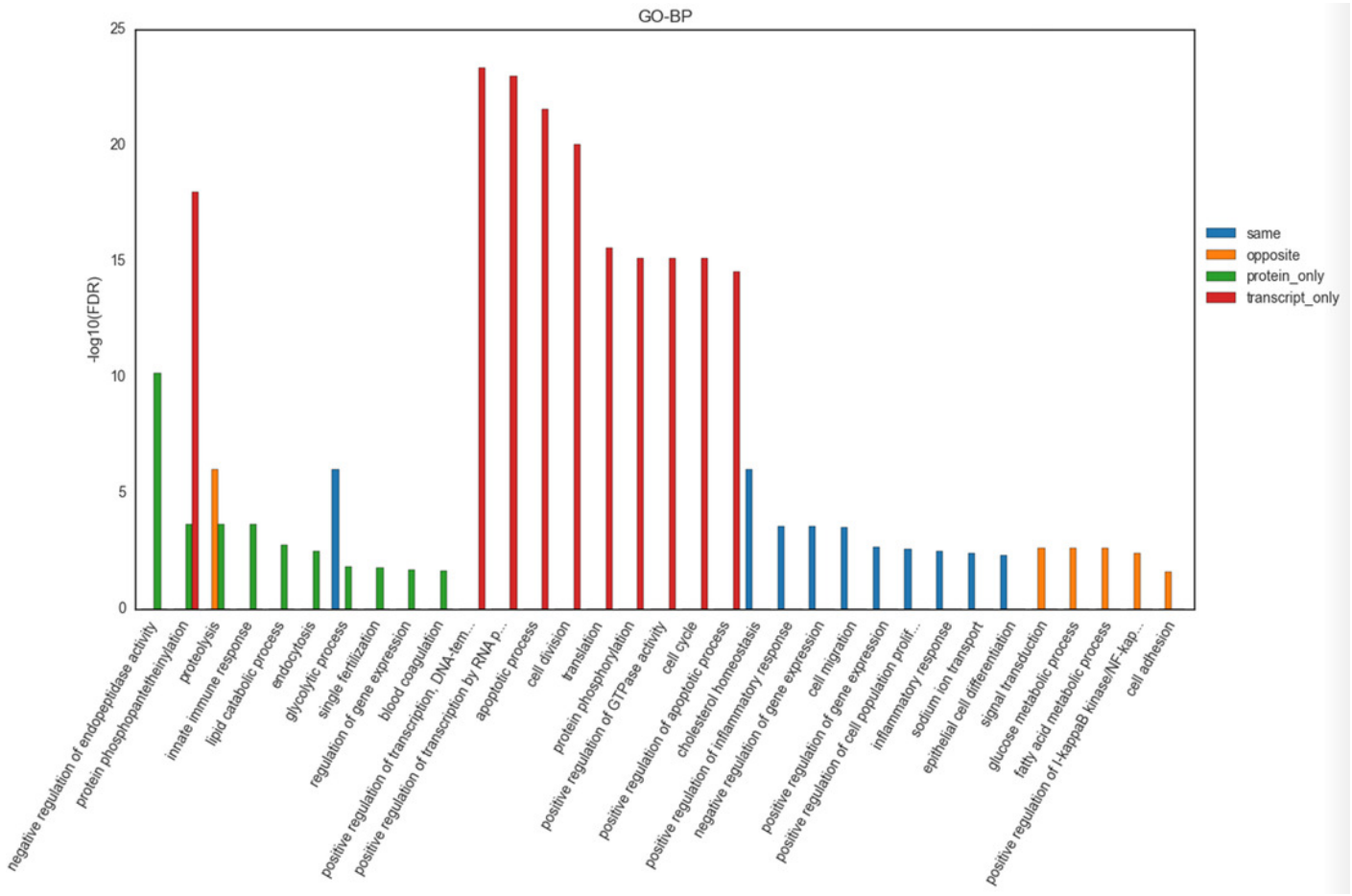

Figure 13

Figure 6E Enrichment associated Pathway

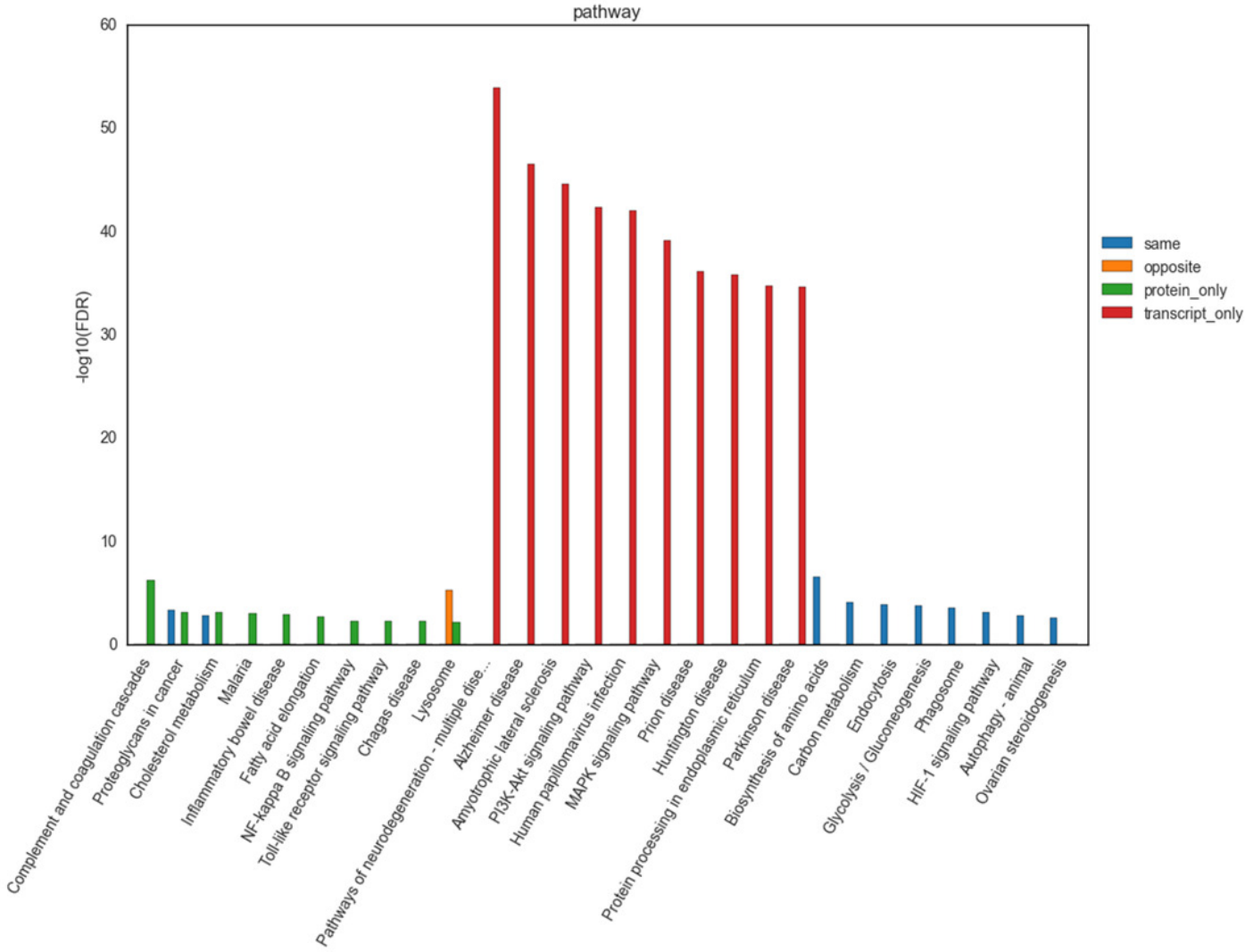

Table 1(on next page)

KEGG list with significantly enriched down-regulated differential genes

1

KEGGID	Description	pvalue	Gene Count
bom00100	Steroid biosynthesis	1.79767583593	10
bom00900	Terpenoid backbone biosynthesis	1.6593635985	8
bom01212	Fatty acid metabolism	0.0000237145601294849	8
bom03320	PPAR signaling pathway	0.00037975	7
bom04216	Ferroptosis	0.000773436	7

Table 2(on next page)

KEGG list with significantly enriched upregulated differential genes

1

KEGGID	Description	pvalue	Gene Count
bom04080	Neuroactive ligand-receptor interaction	6.8077128097	18
bom05032	Morphine addiction	3.616289593935	11
bom05150	Staphylococcus aureus infection	0.000649041	6
bom04512	ECM-receptor interaction	0.000897743	8
bom00350	Tyrosine metabolism	0.001010165	5
bom00360	Phenylalanine metabolism	0.001074598	4

Table 3(on next page)

Information of primers for RT- qPCR

1

Gene	Primer sequence		Prodict length (bp)
ACTB	F:TCATCACCATCGGCAATGAG	R:AGCACCGTGTTGGCGTAGAG	157
FGFR2	F:ACGGGTCCATCAATCATACG	R:AACTCCACATCGCCTCCAAC	118
IL6	F:ACCACCCCAGGCAGACTACT	R:ATTGAACCCAGATTGGAAGC	204
OSMR	F:ACTGCCTTCCTACACTTTAT	R:GTGAGTCTTGAGTTACTTGC	95
PDGFB	F:TAGACCGCACCAATGCTAAC	R:TCTTCCGCACGATCTCAATC	153
FGFR3	F:GATGACGCCACGGATAAGGA	R:CCTAGCAGGTTGATAATGTTCT	95
NTF3	F:ATGTTTCTCGCTTATCTCCG	R:AGGGTGCTCTGGTAGTTCTC	167
EREG	F:ACCTGGTAGACATGAGTGAA	R:CAGCAACTATGACAAGGAAC	156
HMOX1	F:CTGGTGATGGCGTCTTTGTA	R:TCTGGGAAGTAGAGGGGAGT	98
PLCG2	F:TACTTCCCGTCCAATTACGT	R:GTGGGGCTTTTACAACATTA	142
CSF1	F:AGGAGGTGTCGGAGAACTGT	R:GTCTTTGAAGCGCATGGTAT	206
ITGA11	F:GGCGAGCAGATAGGCTCTTA	R:CCACCACATCGTTGTAGGAA	268
SPP1	F:CGATGATGATAACAGCCAGGAC	R:CGTAGGGATAAATGGAGTGAAA	166
PTGS2	F:GTTTTCTGCTGAAGCCCTAT	R:AAAACCTACTTCTCCACCGA	263
THPO	F:GAATTGCTCCTCGTGGTCAT	R:GGAGTCACGAAGCAGTTTATTT	108
FN1	F:GACCGTATCCGCCGAATGTA	R:TTCTGCCTCTGCTGGTCTTT	250
LEP	F:TCCAGGATGACACCAAAACC	R:CAGGGATGAAGTCCAAACCA	114
TLR4	F:GACTGGGTGCGGAATGAACT	R:AACCTTACGGCTTTTGTGGA	144
HIF-1α	F:ATACAGTATTCCAGCCCACT	R:TGTTCTATGACTCCTTTTCC	241
HIF-2α	F:CTCAGGGTCCAGACGTGATG	R:AGGCTTGCTCCTCGTACTCC	90
EPO	F:GAATCTACTCCAATTTCCTGC	R:GAGTTGAGCTCTGGACAGTTC	259
VEGF	F:AGAGCCCCCAGAAGAACGCTC	R:CTTCATCCTGCCCTTGAAACG	81

Table 4(on next page)

Retrotranscriptional reaction system

Reagent	Quantity added per tube
5x RT buffer	5 μl
10 mM dNTPs	2 μl
Rnasin (40 U/μL)	0.5μl
M-MLV-RTase (200 U/μl)	0.5 μl
RNase-Free H2O	6 μl

1

Table 5(on next page)

RT-qPCR reaction system

Reagent	Quantity added per tube
SYBR premix ex taq	6.0 μL
Forward primer (5 μM)	0.5 μL
Downstream primers (5 μM)	0.5 μL
Template (reverse transcription product)	1.0 μL
RNase-Free H2O	4.0 μL

1

Table 6(on next page)

Screening of important DEPs

DEPs name	*P*-value	UP/DOWN	Pathway
PGK	0.00004383995	UP	HIF-1 signaling pathway biosynthesis of secondary metabolites central carbon metabolism in cancer glycolysis/gluconeogenesis
HK	0.00002034812	UP	
LDH	0.00001463732	UP	
PGAM	0.000007788804	UP	
pfkA	0.000002953298	UP	
PDK1	0.00005644263	UP	

1

Table 7 (on next page)

Enrichment analysis results of genes with similar expression trends in proteome and transcriptome

Gene set Name	Description	Genes in overlap	P-value
bta01230	Biosynthesis of amino acids	6	0.0000000008274853
bta01200	Carbon metabolism	5	0.0000005137747
bta04144	Endocytosis	6	0.000001312751
bta00010	Glycolysis / Gluconeogenesis	4	0.000001899059
bta04145	Phagosome	5	0.000004067879
bta05205	Proteoglycans in cancer	5	0.000009315274
bta04066	HIF-1 signaling pathway	4	0.0000164563
bta04140	Autophagy - animal	4	0.0000447763
bta04979	Cholesterol metabolism	3	0.00004547926
bta04913	Ovarian steroidogenesis	3	0.00009097859
bta05230	Central carbon metabolism in cancer	3	0.000114256
bta03320	PPAR signaling pathway	3	0.000213858
bta00100	Steroid biosynthesis	2	0.000342524
bta04152	AMPK signaling pathway	3	0.00065382
bta04977	Vitamin digestion and absorption	2	0.000628869
bta00051	Fructose and mannose metabolism	2	0.000998926
bta00260	Glycine, serine and threonine metabolism	2	0.001745798
bta04216	Ferroptosis	2	0.001745798
bta01523	Antifolate resistance	2	0.002236525
bta04510	Focal adhesion	3	0.002669934
bta04213	Longevity regulating pathway - multiple species	2	0.003285116

1